

1    **August 12, 2021**

2

3    **Toxoplasma bradyzoites exhibit physiological plasticity of calcium and energy**  
4    **stores controlling motility and egress.**

5

6    Yong Fu<sup>1</sup>, Kevin M. Brown<sup>1a</sup>, Nathaniel G. Jones<sup>1b</sup>, Silvia N. J. Moreno<sup>2</sup>, L. David Sibley<sup>1\*</sup>

7    <sup>1</sup>Department of Molecular Microbiology, Washington University in St. Louis, School of Medicine, St Louis,  
8    MO, United States

9    <sup>2</sup>Center for Tropical and Emerging Global Diseases and Department of Cellular Biology, University of  
10   Georgia, Athens, GA, United States

11

12   Running title: *Calcium signaling in bradyzoites*

13   \* Corresponding author

14   E-mail: [sibley@wustl.edu](mailto:sibley@wustl.edu)

15

16   Present addresses

17   <sup>a</sup>Department of Microbiology and Immunology, University of Oklahoma Health Sciences Center, College of  
18   Medicine, Oklahoma City, OK, United States

19   <sup>b</sup>York Biomedical Research Institute, Department of Biology, University of York, Wentworth Way, Heslington,  
20   York, YO10 5DD, U.K.

21

22   **Key words:** tissue cyst, chronic infection, microneme secretion, calcium signaling, calcium ATPases,  
23   exocytosis, motility, dormancy, latency, reactivation

24

25

26

27 **Abstract**

28 *Toxoplasma gondii* has evolved different developmental stages for disseminating during acute infection (i.e.  
29 tachyzoites) and for establishing chronic infection (i.e. bradyzoites). Calcium ion ( $\text{Ca}^{2+}$ ) signaling tightly  
30 regulates the lytic cycle of tachyzoites by controlling microneme secretion and motility to drive egress and  
31 cell invasion. However, the roles of  $\text{Ca}^{2+}$  signaling pathways in bradyzoites remain largely unexplored. Here  
32 we show that  $\text{Ca}^{2+}$  responses are highly restricted in bradyzoites and that they fail to egress in response to  
33 agonists. Development of dual-reporter parasites revealed damped calcium responses and minimal  
34 microneme secretion by bradyzoites induced in vitro or harvested from infected mice and tested ex vivo.  
35 Ratiometric  $\text{Ca}^{2+}$  imaging demonstrated lower  $\text{Ca}^{2+}$  basal levels, reduced magnitude, and slower  $\text{Ca}^{2+}$  kinetics  
36 in bradyzoites compared with tachyzoites stimulated with agonists. Diminished responses in bradyzoites were  
37 associated with down-regulation of calcium ATPases involved in intracellular  $\text{Ca}^{2+}$  storage in the endoplasmic  
38 reticulum (ER) and acidocalcisomes. Once liberated from cysts by trypsin digestion, bradyzoites incubated in  
39 glucose plus calcium rapidly restored their intracellular  $\text{Ca}^{2+}$  and ATP stores leading to enhanced gliding.  
40 Collectively, our findings indicate that intracellular bradyzoites exhibit damped  $\text{Ca}^{2+}$  signaling and lower  
41 energy levels that restrict egress, and yet upon release they rapidly respond to changes in the environment to  
42 regain motility.

43

44 **Introduction**

45 *Toxoplasma gondii* is an obligate intracellular parasite, capable of infecting nearly all warm-blooded  
46 animals and frequently causing human infections [1]. The ingestion of tissue cysts in undercooked meat or  
47 shed oocysts by infected cats are the major transmission routes of *T. gondii* [2,3]. Following oral ingestion of  
48 bradyzoites within tissue cysts or sporozoites within oocysts, the parasite migrates across the intestinal  
49 epithelial barrier and disseminates throughout the body as the actively proliferating tachyzoite form that  
50 infects many cell types but primarily traffics in monocytes [4]. In response to immune pressure, the parasite  
51 differentiates to asynchronously growing bradyzoites within cysts that can persist as chronic infections in  
52 muscle and brain tissues [5-7].

53 Tachyzoites are adapted for rapid proliferation and dissemination due to an active lytic cycle that is  
54 controlled at numerous stages by intracellular calcium ion ( $\text{Ca}^{2+}$ ) signaling [8]. Artificially elevating  
55 intracellular  $\text{Ca}^{2+}$  using ionophores triggers secretion of microneme proteins, which are needed for substrate  
56 and cell attachment, and hence critical for both gliding motility and cell invasion [9-11]. Increase of cytosolic  
57  $\text{Ca}^{2+}$  released from internal stores is sufficient to trigger microneme secretion [12], and necessary for host cell  
58 invasion [12,13], although these processes are also enhanced by the presence of extracellular  $\text{Ca}^{2+}$  [14].  
59 Increases in intracellular  $\text{Ca}^{2+}$  also precede egress and drive secretion of perforin like protein 1 (PLP1) from  
60 microneme to facilitate rupture of parasitophorous vacuole membrane (PVM) followed by egress [15].  
61 Calcium signaling is initiated by cyclic guanosine monophosphate (cGMP)-generating guanylate cyclase (GC)  
62 [16-18] that activates parasite plasma membrane-associated protein kinase G (PKG) [19], stimulating the  
63 production of inositol triphosphate ( $\text{IP}_3$ ) by phosphoinositide-phospholipase C (PI-PLC) and leading to  
64 subsequent release of intracellular  $\text{Ca}^{2+}$  [12,20,21]. Recent studies in *Plasmodium* also implicate PKG in  
65 directly controlling calcium through interaction with a multimembrane spanning protein that may function as

66 a channel that mediates calcium release [22]. In turn,  $\text{Ca}^{2+}$  activates downstream  $\text{Ca}^{2+}$  responsive proteins  
67 including  $\text{Ca}^{2+}$  dependent protein kinases such as CDPK1 [8] and CDPK3 [23,24], and C2 domain-containing  
68  $\text{Ca}^{2+}$  binding proteins [25], and calcium binding orthologues of calmodulin [26], which are required for  
69 invasion and egress by tachyzoites. Following invasion, protein kinase A catalytic domain 1 (PKAc1)  
70 dampens cytosolic  $\text{Ca}^{2+}$  by suppressing cGMP signaling and reducing  $\text{Ca}^{2+}$  uptake [27,28]. Collectively, the  
71 lytic life cycle of tachyzoites is orchestrated spatially and temporally by controlling levels of intracellular  $\text{Ca}^{2+}$   
72 and cyclic nucleotides [29].

73 *Toxoplasma* has evolved elaborate mechanism to control intracellular  $\text{Ca}^{2+}$  levels through the concerted  
74 action of calcium channels, transporters, and  $\text{Ca}^{2+}$  pumps expressed at the PM and intracellular stores [8,30].  
75 Orthologues to voltage-dependent  $\text{Ca}^{2+}$  channels, transient receptor potential (TRP) channels, and plasma  
76 membrane type  $\text{Ca}^{2+}$ -ATPases (PMCA) are predicted to be present in *T. gondii* and likely involved in  
77 regulating cytosolic  $\text{Ca}^{2+}$  influx and efflux [31,32]. The endoplasmic reticulum (ER) is the most important  
78 storage site from which  $\text{Ca}^{2+}$  is released to stimulate motility and egress of *Toxoplasma* [8]. SERCA-type  $\text{Ca}^{2+}$   
79 ATPase is the known mechanism for  $\text{Ca}^{2+}$  uptake by the ER and its activity, which is inhibited by thapsigargin  
80 [33], leads to accumulation of  $\text{Ca}^{2+}$  in the ER, which when released activates microneme secretion and  
81 motility [34,35]. TgA1 a plasma membrane type  $\text{Ca}^{2+}$  ATPase, transport  $\text{Ca}^{2+}$  to the acidocalcisome [36],  
82 which likely provides a  $\text{Ca}^{2+}$  sink albeit one that may not be as readily mobilizable as the ER. In addition to  
83 internal  $\text{Ca}^{2+}$  stores, intracellular and extracellular *T. gondii* tachyzoites are capable of taking up  $\text{Ca}^{2+}$  from  
84 host cells and the extracellular environment, respectively, to enhance  $\text{Ca}^{2+}$  signaling pathways [14,37]. A  
85 variety of fluorescent  $\text{Ca}^{2+}$  indicators that have been developed to directly image  $\text{Ca}^{2+}$  signals in live cells  
86 include  $\text{Ca}^{2+}$  responsive dyes and genetically encoded indicators [38]. Indicators like Fluo-4/AM, and related  
87 derivatives, have been previously used to monitor  $\text{Ca}^{2+}$  levels in extracellular parasites [34,39]. Genetically  
88 encoded calcium indicators such as GCaMP5, GCaMP6f and GCaMP7 have also been used to visualize  
89 dynamic  $\text{Ca}^{2+}$  signals of both intracellular and extracellular tachyzoites with high resolution and sensitivity  
90 [37,40-42].

91 In contrast to tachyzoites, little is known about the roles of  $\text{Ca}^{2+}$  signaling in control of microneme  
92 secretion, gliding motility, and egress by bradyzoites. Although bradyzoites divide asynchronously, they  
93 undergo growth, expansion, and sequential rounds of tissue cyst formation and rupture that maintain chronic  
94 infection *in vivo* [5]. Histological studies in animal models support a model of periodic cyst rupture [43],  
95 releasing bradyzoites that reinvoke new host cells to generate secondary daughter cysts [44], or transition back  
96 to actively replicating tachyzoites [45]. Development of bradyzoites has been studied *in vitro* using systems  
97 that induce development due to stress induced by alkaline pH [46] or in cell lines where development occurs  
98 spontaneously [47,48]. Although numerous studies have focused on the determinants that control stage  
99 conversion between tachyzoites and bradyzoites [6,49], few studies focus on the signaling pathways that  
100 control the bradyzoite lytic cycle.

101 In the present study, we combined stage-specific bradyzoite fluorescent reporters with  $\text{Ca}^{2+}$  imaging  
102 probes to explore  $\text{Ca}^{2+}$  signaling, microneme secretion, motility and egress by bradyzoites. Our findings  
103 indicate that bradyzoites exhibit dampened  $\text{Ca}^{2+}$  levels, reduced microneme secretion, and minimal egress in  
104 response to  $\text{Ca}^{2+}$  agonists. Ratiometric  $\text{Ca}^{2+}$  imaging demonstrated lower  $\text{Ca}^{2+}$  basal levels and significantly

105 lower stored  $\text{Ca}^{2+}$  in ER and acidocalcisome in bradyzoites, associated with reduced expression of  $\text{Ca}^{2+}$   
106 ATPases responsible for maintaining intracellular stores. Incubation of extracellular bradyzoites in  $\text{Ca}^{2+}$  plus  
107 glucose lead to rapid recover of both intracellular  $\text{Ca}^{2+}$  and ATP levels and restored motility. Collectively our  
108 findings support a dampened lytic cycle in bradyzoites, arising from diminished  $\text{Ca}^{2+}$  signaling and lowered  
109 energy stores, and that upon release they exhibit rapid metabolic responsiveness to environmental conditions.  
110

## 111 **Results**

### 112 **$\text{Ca}^{2+}$ signaling triggers inefficient egress by bradyzoites**

113 To define egress by bradyzoites, we induced the differentiation of tachyzoites to bradyzoites by culture in  
114 HFF cells at alkaline pH (8.2) for 7 days. We treated both tachyzoite cultures and in vitro differentiated cysts  
115 with  $\text{Ca}^{2+}$  ionophore A23187 to trigger egress from parasitophorous vacuoles (PVs) or bradyzoite cysts, as  
116 detected by indirect immunofluorescence assay (IFA) or time lapse video microscopy. We observed that  
117 A23187 induced complete egress of tachyzoites from disrupted PVs while only few bradyzoites were released  
118 from cysts that remained largely intact (**Figure 1A**). This result was also confirmed by time-lapse video  
119 microscopy using the ME49 BAG1-mCherry strain either grown as tachyzoites (**Figure 1-video 1**) or  
120 bradyzoites (**Figure 1-video 2**). We quantified the percentage of tachyzoites or bradyzoites that were released  
121 during egress in response to A23187 or the agonist zaprinast, which is a cGMP specific phosphodiesterase  
122 (PDE) inhibitor that activates PKG-mediated  $\text{Ca}^{2+}$  signaling, leading to egress. In contrast to tachyzoites, we  
123 found significantly lower egress rate of bradyzoites in response to A23817 or zaprinast (**Figure 1B**). To  
124 examine the behavior of released parasites, we determined the maximum egress distance that parasites moved  
125 away from the original vacuole or cyst following egress. Tachyzoites migrated much further than bradyzoites  
126 after induced egress (**Figure 1C**). Bradyzoites also moved more slowly than tachyzoites (**Figure 1D**), as  
127 shown by quantification of their trajectories from time lapse video microscopy images. Taken together, these  
128 findings indicate that egress by bradyzoites in response to  $\text{Ca}^{2+}$  ionophore or zaprinast is incomplete and  
129 restricted.  
130

### 131 **Calcium-mediated microneme secretion is dampened by bradyzoite development**

132 Egress by parasites requires  $\text{Ca}^{2+}$ -stimulated microneme secretion. To examine the reason for inefficient  
133 egress by bradyzoites, we monitored microneme secretion by quantitative secretion analysis of MIC2 fused  
134 with *Gaussia Luciferase* (Gluc). The *MIC2-Gluc* reporter was randomly integrated into the genome of the  
135 BAG1-mCherry strain (**Figure 2A**). IFA revealed that MIC2-Gluc was expressed and localized to  
136 micronemes in tachyzoites and bradyzoites induced for 7 days at pH 8.2 in vitro, as confirmed by expression  
137 of BAG1-mCherry (**Figure 2B**). BAG1-mCherry MIC2-GLuc strain tachyzoites, and bradyzoites liberated  
138 from cysts produced by cultivation for 7 days at pH 8.2 in vitro, were sorted by FACS (**Figure 2C**). FACS  
139 sorted tachyzoites and bradyzoites were treated with zaprinast or ionomycin, a  $\text{Ca}^{2+}$  ionophore that induces  
140 release of  $\text{Ca}^{2+}$  from the ER [50]. Bradyzoites secreted much less MIC2-Gluc protein compared to tachyzoites  
141 in response to  $\text{Ca}^{2+}$  agonists, zaprinast and ionomycin as shown by *Gaussia luciferase* assays performed on  
142 ESA fractions collected following stimulation (**Figure 2D**). To further investigate the process of microneme  
143 secretion by bradyzoites, we randomly integrated a mCherry secretion reporter, based on the signal peptide

144 sequence of ferredoxin-NADP(+) -reductase (FNR-mCherry), into the genome of BAG1-EGFP parasites  
145 (**Figure 2E**). The FNR-mCherry reporter is an improved version of DsRed reporter that is secreted into the  
146 matrix of PV, and released following the discharge of PLP1 in response to  $\text{Ca}^{2+}$  agonists [15]. Then we  
147 monitored the permeabilization of PV membrane or cyst wall after stimulation with A23187 based on the  
148 diffusion of FNR-mCherry using time-lapse fluorescence video microscopy. Consistent with previous reports  
149 [51], we observed that A23187 stimulated fast leakage of FNR-mCherry from the PV surrounding tachyzoites  
150 (**Figure 2F**, top panel and **Figure 2-video 1**). However, FNR-mCherry was not released from the cyst after  
151 A23187 stimulation (**Figure 2F**, middle panel and **Figure 2-video 3**). As a control to confirm that the  
152 FNR-mCherry was indeed secreted into the lumen of the cyst matrix, we treated cysts with trypsin to release  
153 bradyzoites. Once the cyst wall was digested, the FNR-mCherry dissipated rapidly, confirming that it was  
154 present in the matrix of the cyst (**Figure 2F**, bottom panel and **Figure 2-video 2**). These data were also  
155 confirmed by plotting FNR-mCherry fluorescence intensity changes vs. time for tachyzoites vs. intact or  
156 trypsin treated cysts (**Figure 2G**). These findings demonstrate dampened microneme secretion by bradyzoites,  
157 which may explain their incomplete egress.

158

#### 159 **Genetically encoded calcium reporter reveals dampened $\text{Ca}^{2+}$ responses in bradyzoites**

160 To investigate  $\text{Ca}^{2+}$  signaling in bradyzoites, we established a dual fluorescent reporter system containing  
161 constitutively expressed GCaMP6f and mCherry under the control of bradyzoite stage-specific promoter  
162 BAG1 (**Figure 3A**). Using this system, both tachyzoites and bradyzoites express the same levels of GCaMP6f,  
163 while only bradyzoites express mCherry, allowing specific monitoring of  $\text{Ca}^{2+}$  signals in both stages. We  
164 compared the response of BAG1-mCherry GCaMP6f reporter parasites that were grown as tachyzoites, to  
165 those induced to form bradyzoites by cultivation in HFF cells for 7 days at pH 8.2 in vitro, after treatment  
166 with  $\text{Ca}^{2+}$  ionophore A23187. A23187 induced rapid and high-level increases in GCaMP6f fluorescence in  
167 tachyzoites but delayed and much weaker responses in bradyzoites as monitored by time-lapse video  
168 microscopy (**Figure 3B**, **Figure 3-video 1** and **Figure 3-video 2**). To determine the effect of bradyzoite  
169 development on  $\text{Ca}^{2+}$  signaling, we treated intracellular tachyzoites, vs. bradyzoites induced by cultivation in  
170 HFF cells at pH 8.2 in vitro for 4 to 7 days, and quantified time of each tachyzoite vacuole or bradyzoite cyst  
171 to reach  $\text{Ca}^{2+}$  peak level after addition of A23187 ionophore by video microscopy. Increasing time of  
172 bradyzoites development was associated with progressively longer times to reach peak fluorescence of  
173 GCaMP6f (**Figure 3C**). Time lapse recording of GCaMP6f fluorescence intensity ratio changes ( $F/F_0$ ) showed  
174 delayed  $\text{Ca}^{2+}$  increase and lower fold changes in bradyzoites compared with tachyzoites in response to  
175 A23187 stimulation (**Figure 3D**). Zaprinast also elicited slower  $\text{Ca}^{2+}$  increases and lower fold changes in  
176 bradyzoites compared with tachyzoites even in the presence of extracellular  $\text{Ca}^{2+}$  (**Figure 3E**). To better  
177 characterize  $\text{Ca}^{2+}$  responses of bradyzoites, we performed live video imaging using spinning disc confocal  
178 microscopy to distinguish individual bradyzoites within in vitro differentiated cysts and identify motile  
179 bradyzoites within cysts by comparing consecutive images (**Figure 3F**). Motile bradyzoites were also  
180 observed to have higher GCaMP6f signals and these typically oscillated over time. In response to  $\text{Ca}^{2+}$   
181 agonists, intracellular bradyzoites showed reduced percentages of motility compared to tachyzoites (**Figure**  
182 **3G**). In summary,  $\text{Ca}^{2+}$  dynamics are delayed and reduced in bradyzoites in response to  $\text{Ca}^{2+}$  agonists.

183

184 **Bradyzoites formed in skeletal muscle cell and within ex vivo cysts show diminished  $\text{Ca}^{2+}$  responses**

185 To rule out the possibility that alkaline pH stress used for differentiation resulted in lowered  $\text{Ca}^{2+}$  signals in  
186 bradyzoites, we examined  $\text{Ca}^{2+}$  signaling in bradyzoites within cysts that formed naturally in differentiated  
187 C2C12 myocytes. Differentiated myocytes stained positively for skeletal myosin, and facilitated the  
188 development of bradyzoites, as shown using the bradyzoite stage-specific protein BAG1 (**Figure 4A**). We  
189 tested  $\text{Ca}^{2+}$  responses of bradyzoites formed in muscle cells using the dual fluorescent reporter GCaMP6f  
190 BAG1-mCherry parasites in response to A23187 or zaprinast by time-lapse video recording. Time-lapse  
191 imaging showed slow increase of GCaMP6f fluorescence in response to A23187 in tissue cysts formed in  
192 C2C12 myocytes (**Figure 4B**). Both the rate of increase and the maximum amplitude of the GCaMP6f signal  
193 was much lower in bradyzoites differentiated in myocytes compared to tachyzoites cultured in  
194 undifferentiated myoblasts (**Figure 4C**). The time to reach the peak GCaMP6f fluorescence was also delayed  
195 in bradyzoites formed in C2C12 myocytes compared with tachyzoites grown in myoblasts (**Figure 4D**).  
196 Bradyzoites cultured in C2C12 myocytes show significantly lower motility in response to A23187 and  
197 zaprinast when compared with tachyzoites (**Figure 4E**).

198 To further examine  $\text{Ca}^{2+}$  signaling in bradyzoites, we harvested tissue cysts containing BAG1-mCherry  
199 GCaMP6f bradyzoites from the brains of chronically infected CD-1 mice and investigated their responses ex  
200 vivo. Video microscopy of ex vivo tissue cysts showed slow increases in GCaMP6f fluorescence in response  
201 to A23187 or zaprinast (**Figure 4F**). The ratio of GCaMP6f fluorescence changes vs time ( $F/F_0$ ) from  
202 bradyzoites within ex vivo cysts demonstrated lower and slower changes, consistent with lower  $\text{Ca}^{2+}$  levels,  
203 compared with extracellular tachyzoites in response to  $\text{Ca}^{2+}$  agonists (**Figure 4G**). In comparing the response  
204 of extracellular, ex vivo tissue cysts (**Figure 4 F,G**) to intracellular cysts formed during infection of C2C12  
205 myocytes (**Figure 4 B,C**), it was evident that the extracellular cysts respond somewhat faster, albeit still much  
206 slower than tachyzoites. This intermediate level of response was also seen in in vitro differentiated tissue cyst  
207 (produced by cultivation in HFF cells at pH 8.2 for 7 days) that were liberated from HFF cells and tested in  
208 vitro (**Figure 4-supplement 1**). Next, we measured the percentage of motile and egressed bradyzoites within  
209 ex vivo tissue cyst treated with A23187 and zaprinast. Strikingly, no egressed bradyzoites were observed  
210 although all the bradyzoites within ex vivo cysts became motile after stimulation (**Figure 4H, Figure 4-video**  
211 **1, Figure 4-video 2**). Taken together, these findings indicate that bradyzoites formed spontaneously in muscle  
212 myocytes and within ex vivo cysts from chronically infected mice display dampened  $\text{Ca}^{2+}$  dynamics when  
213 treated with  $\text{Ca}^{2+}$  agonists.

214

215 **Bradyzoites store less  $\text{Ca}^{2+}$  in ER and acidocalcosome**

216 The cyst wall surrounding bradyzoites may restrict access to  $\text{Ca}^{2+}$  agonists and hence dampen signals from  
217 GCaMP6f in response to  $\text{Ca}^{2+}$  agonists in the studies described above. To test this possibility, we monitored  
218 GCaMP6f fluorescence changes in extracellular bradyzoites vs. tachyzoites of the BAG1-mCherry GCaMP6f  
219 strain by live imaging. Bradyzoites were induced by cultivation in HFF cells at pH 8.2 for 7 days and liberated  
220 from cysts by trypsin treatment, followed by washing and resuspension for analysis. We also observed slower  
221 increases in GCaMP6f fluorescence intensity in bradyzoites (**Figure 5-video 2**) compared with tachyzoites

222 (**Figure 5-video 1**) in response to A23187 (**Figure 5A**). Quantitative analysis of  $\text{Ca}^{2+}$  fluorescence changes  
223 ( $\text{F}/\text{F}_0$ ) after stimulation by A23187 and zaprinast showed slower  $\text{Ca}^{2+}$  responses in extracellular bradyzoites  
224 when compared to tachyzoites (**Figure 5B**). To confirm that extracellular bradyzoites were viable after  
225 liberation from in vitro cultured cysts by trypsin treatment, we utilized SYTOX Red, which is a DNA dye  
226 excluded by intact membranes of viable cells. In contrast to bradyzoites that were formaldehyde-fixed as a  
227 positive control, extracellular bradyzoites were not stained by SYTOX after the liberation from in vitro cysts  
228 (**Figure 5C**), indicating they were still viable after trypsin treatment.

229 We hypothesized that bradyzoites might have dampened GCaMP6f responses because they fail to release  
230  $\text{Ca}^{2+}$  from intracellular stores. We tested  $\text{Ca}^{2+}$  responses of BAG1-mCherry and GCaMP6f -expressing  
231 bradyzoites and tachyzoites treated with ionomycin, which releases  $\text{Ca}^{2+}$  mainly from the ER [50],  
232 thapsigargin, which inhibits SERCA-type  $\text{Ca}^{2+}$ -ATPase causing an increase of cytosolic  $\text{Ca}^{2+}$  due to  
233 uncompensated leakage from the ER [33], and  $\text{NH}_4\text{Cl}$ , an alkalinizing reagent that releases  $\text{Ca}^{2+}$  from acidic  
234 stores like acidocalcisomes [35]. Both ionomycin and thapsigargin induced delayed and lower amplitude  
235 changes in GCaMP6f fluorescence in bradyzoites vs. tachyzoites as shown by plotting fluorescence intensity  
236 fold changes ( $\text{F}/\text{F}_0$ ) vs. time (**Figure 5D**), indicative of lower ER stored  $\text{Ca}^{2+}$ . In contrast, bradyzoites treated  
237 with  $\text{NH}_4\text{Cl}$  showed no meaningful change in GCaMP6f fluorescence, suggesting they lack mobilizable acidic  
238  $\text{Ca}^{2+}$  (**Figure 5D**). To rule out the possibility that the  $\text{Ca}^{2+}$  indicator GCaMP6f is less sensitive in bradyzoites  
239 due to some intrinsic defect, we loaded BAG1-mCherry expressing tachyzoite or bradyzoites with the  $\text{Ca}^{2+}$   
240 sensitive vital dye Fluo-8 AM and used these cells for imaging. Fluo-8 AM labeled bradyzoites displayed  
241 dampened  $\text{Ca}^{2+}$  signaling after stimulation by ionomycin, thapsigargin or  $\text{NH}_4\text{Cl}$ , relative to tachyzoites that  
242 responded normally (**Figure 5E**). Collectively, these findings indicate that bradyzoites are less able to  
243 mobilize  $\text{Ca}^{2+}$  from the ER and acidic stores in response to agonists.

244

#### 245 **Ratiometric sensor reveals reduced basal levels of $\text{Ca}^{2+}$ and dynamics in bradyzoites**

246 To more precisely compare  $\text{Ca}^{2+}$  levels in tachyzoites and bradyzoites, we constructed a ratiometric  
247 fluorescence reporter by co-expression of GCaMP6f with blue fluorescent protein mTagBFP2 linked by a P2A  
248 split peptide (**Figure 6A**, **Figure 6 Supplement 1A**, **Figure 6 Supplement 1B**). Because both proteins are  
249 co-expressed from the same promoter, the mTagBFP2 serves as a control for expression level, as mTagBFP2  
250 is non-responsive to  $\text{Ca}^{2+}$  levels [52]. Live fluorescence microscopy showed simultaneous expression of  
251 GCaMP6f and mTagBFP2 in tachyzoites, and additionally mCherry in bradyzoites (**Figure 6B**). Equal  
252 expression of GCaMP6f (His tag) and mTagBFP2, as well as separation of tachyzoites and bradyzoite  
253 populations (detected with SAG1 and BAG1 respectively) was validated by western blotting (**Figure 6C**). To  
254 compare  $\text{Ca}^{2+}$  basal levels, we quantified the fluorescence intensity ratio  $\text{F}_{\text{GCaMP6f}}/\text{F}_{\text{mTagBFP2}}$  of intracellular and  
255 extracellular tachyzoites and bradyzoites in EC buffer with or without  $\text{Ca}^{2+}$ . We observed significant  
256 reductions in the fluorescence intensity ratio of both intracellular and extracellular bradyzoites relative to  
257 tachyzoites (**Figure 6D**), indicative of lower resting  $\text{Ca}^{2+}$  levels in bradyzoites. We next compared  $\text{Ca}^{2+}$   
258 dynamics of intracellular tachyzoites and bradyzoites in response to  $\text{Ca}^{2+}$  agonists ionomycin,  $\text{NH}_4\text{Cl}$  and  
259 thapsigargin. Changes in the fluorescence of GCaMP6f were much slower and of lower amplitude in  
260 bradyzoites relative to tachyzoites (**Figure 6E**). We also observed lower resting  $\text{Ca}^{2+}$  and peak levels in

261 extracellular bradyzoites compared to tachyzoites (**Figure 6F**), indicating lower activity or expression of  
262 cytoplasmic influx mechanisms like the PM entry or ER release channels. To understand the molecular basis  
263 for the reduced stored  $\text{Ca}^{2+}$  and responses in bradyzoites, we performed real-time PCR to compare mRNA  
264 expression levels of TgSERCA [34], which is the drug target of thapsigargin and transfers  $\text{Ca}^{2+}$  from the  
265 cytosol of parasites to ER, TgA1 [36], which plays important roles in the accumulation of  $\text{Ca}^{2+}$  in the  
266 acidocalcisome and other acidic stores, TgTRPPL-2 [53], which is a transient receptor potential (TRP)  
267 channel key for  $\text{Ca}^{2+}$  influx into the cytosol, and other calcium-related proteins, such as TgPMCA1, TgA2 and  
268 the  $\text{Ca}^{2+}/\text{H}^+$  exchanger [54]. We observed significant reduction in the relative expression level of TgSERCA,  
269 TgA1, TgPMCA1, TgA2,  $\text{Ca}^{2+}/\text{H}^+$  exchanger and TgTRPPL-2 in bradyzoites compared to tachyzoites (**Figure**  
270 **6G**). Taken together, these findings indicate that bradyzoites have lower levels of stored  $\text{Ca}^{2+}$ , which is  
271 associated with the overall downregulation of  $\text{Ca}^{2+}$ -related pumps and channels.

272

### 273 **Calcium signaling plays a critical role in gliding motility of bradyzoites**

274 To test whether dampened  $\text{Ca}^{2+}$  signaling would still be sufficient to drive gliding motility of bradyzoites, we  
275 treated BAG1-mCherry GCaMP6f expressing cysts cultured in vitro with trypsin to liberate bradyzoites  
276 (**Figure 7A**). There were no obvious changes in the  $\text{Ca}^{2+}$  levels nor motility during trypsin treatment and  
277 release (**Figure 7B** and **Figure 7-video 1**). When we monitored the motility of released bradyzoites by  
278 time-lapse video microscopy, a number of bradyzoites underwent circular gliding (**Figure 7C** and **Figure**  
279 **7-video 2**) in patterns that were highly reminiscent of tachyzoite motility. Similar to previous descriptions of  
280 oscillating  $\text{Ca}^{2+}$  patterns in gliding tachyzoites [39], we observed fluctuations of GCaMP6f fluorescence  
281 intensities in single extracellular bradyzoites with gliding motility (**Figure 7D**).

282 To further characterize the role of  $\text{Ca}^{2+}$  signaling in bradyzoites motility, we treated cells with the  $\text{Ca}^{2+}$   
283 chelator BAPTA-AM, the PKG inhibitor compound 1, and the CDPK1 inhibitor 3-MB-PP1 to block  $\text{Ca}^{2+}$   
284 signaling in bradyzoites. All these inhibitors significantly impaired gliding motility of tachyzoites and  
285 bradyzoites (**Figure 7E** and **Figure 7F**), confirming a key role of  $\text{Ca}^{2+}$  signaling in parasite motility.  
286 Bradyzoites displayed shorter gliding distance compared with tachyzoites as determined by measurements of  
287 trail lengths detected with SAG1 (tachyzoite) or SRS9 (bradyzoites) (**Figure 7F**). In summary, despite having  
288 dampened  $\text{Ca}^{2+}$  stores and reduced responses to agonist when intracellular, extracellular bradyzoites require  
289 calcium signaling to activate gliding motility.

290

### 291 **Accumulation of calcium stores and ATP synergistically activates gliding motility by bradyzoites**

292 Following reactivation of tissue cysts, we hypothesize that bradyzoites must replenish their  $\text{Ca}^{2+}$  and energy  
293 stores to meet the demands of cell to cell transmission. To test this idea, we released bradyzoites using trypsin  
294 treatment and then treated extracellular bradyzoites with EC buffer with or without  $\text{Ca}^{2+}$  (1.8 mM) and with or  
295 without glucose (5.6 mM) for different times and stimulated the calcium responses using ionomycin.  
296 Quantitative analysis of  $\text{Ca}^{2+}$  fluorescence changes ( $F/F_0$ ) showed that bradyzoites recovered substantial stored  
297  $\text{Ca}^{2+}$  in the presence of exogenous  $\text{Ca}^{2+}$  and glucose for 1 hr compared to 10 min (**Figure 8A and 8B**). A more

298 modest recovery was observed in the presence of  $\text{Ca}^{2+}$  but absence of glucose (**Figure 8B**). Next, we  
299 investigated the effect of exogenous  $\text{Ca}^{2+}$  and glucose on gliding motility by bradyzoites. We used time-lapse  
300 video microscopy to determine the percentage of extracellular bradyzoites undergoing twirling, circular and  
301 helical motility after incubation in EC buffer  $\pm \text{Ca}^{2+}$  and glucose for 10 min vs 1 hr. Quantitative analysis  
302 showed that bradyzoites underwent all forms of gliding motility and substantially recovered gliding motility  
303 after incubation with EC buffer containing both  $\text{Ca}^{2+}$  and glucose for 1 hr, while very few bradyzoites were  
304 able to glide following incubation with exogenous  $\text{Ca}^{2+}$  or glucose alone (**Figure 8C**).

305 We reasoned that exogenous glucose could be utilized by parasites to produce ATP via glycolysis or  
306 oxidative phosphorylation to maintain a variety of cellular functions. To investigate the ATP source for  
307 supporting gliding motility, we treated exogenous bradyzoites in EC buffer containing  $\text{Ca}^{2+}$  (1.8 mM) with  
308 glucose to support glycolysis vs. the glucose analogue 2-deoxy-D-glucose (2-DOG) to block glycolysis  
309 (**Figure 8D**). Alternatively, similar preparations of bradyzoites were incubated with glutamine to provide  
310 substrates for the tricarboxylic acid (TCA) cycle or the ATP synthase inhibitor oligomycin A to inhibit  
311 oxidative phosphorylation (**Figure 8D**). Quantitative analysis of percentage of gliding motility showed either  
312 glucose or glutamine significantly increased gliding motility by bradyzoites (**Figure 8E**), indicating that either  
313 carbon source can be used to produce ATP for maintaining gliding motility. Either 2-DOG or oligomycin A  
314 blocked gliding motility by bradyzoites even in the presence of exogenous glucose or glutamine (**Figure 8E**),  
315 demonstrating that both oxidative phosphorylation and glycolysis are ATP sources for driving gliding motility  
316 by bradyzoites.

317 To further investigate the energy status of bradyzoites, we utilized reversed-phase high-performance  
318 liquid chromatography (RP-HPLC) to measure the adenosine triphosphate (ATP), adenosine diphosphate  
319 (ADP) and adenosine monophosphate (AMP) levels in bradyzoites treated with EC buffer containing both  
320  $\text{Ca}^{2+}$  (1.8 mM) and glucose (5.6 mM) for different time (**Figure 8-supplement 1A, 1B and 1C**). We observed  
321 that after the incubation in EC buffer for 1 hr, bradyzoites had significantly higher ATP, ADP and AMP levels  
322 (**Figure 8F**), demonstrating enhanced ATP production during incubation. The ATP/ADP ratio and energy  
323 charge have been widely used to evaluate cellular energy status, which controls the free-energy change for  
324 ATP hydrolysis for different cellular functions [55]. Bradyzoites incubated with EC buffer for 1 hr displayed  
325 significantly increased ATP/ADP ratio and energy charge (**Figure 8G and 8H**), indicating bradyzoites rapidly  
326 recover their energy status following incubation with glucose. Collectively, exogenous  $\text{Ca}^{2+}$  and glucose  
327 altogether activate bradyzoite gliding motility via restoration of ATP levels and  $\text{Ca}^{2+}$  stores.

## 328 Discussion

329 Calcium signaling plays important roles in the control of microneme secretion, gliding motility, and egress  
330 of apicomplexan parasites and these pathways have been extensively characterized in the tachyzoite stage of *T.*  
331 *gondii* [8,30], although not widely explored in other motile life cycle stages. Here we compared the responses  
332 of *T. gondii* tachyzoites and bradyzoites to  $\text{Ca}^{2+}$  ionophores and agonists that cause release of  $\text{Ca}^{2+}$  from  
333 intracellular stores and found that  $\text{Ca}^{2+}$  responses, microneme secretion, and egress by bradyzoites were all  
334 highly attenuated. Dampened  $\text{Ca}^{2+}$  responses were evident in the responses of in vitro cysts differentiated

335 under stress conditions, naturally occurring cysts formed in muscle cells, and tissue cysts purified from brains  
336 of chronically infected mice and tested ex vivo. Reduced responses were not simply a consequence of the  
337 intracellular environment, as similar damped  $\text{Ca}^{2+}$  signals and microneme secretion were observed in single,  
338 extracellular bradyzoites. Ratiometric  $\text{Ca}^{2+}$  imaging revealed lower resting  $\text{Ca}^{2+}$  levels and reduced ER and  
339 acidic stored  $\text{Ca}^{2+}$  in bradyzoites, which is likely a reflection of down-regulation of  $\text{Ca}^{2+}$ -ATPases involved in  
340 maintaining these stores replenished. Tissue cysts are characterized by a thick wall comprised of proteins and  
341 carbohydrates which may collectively impede signals and/or restrict egress mechanically. However, when  
342 cysts were digested by trypsin to release bradyzoites, they exhibited  $\text{Ca}^{2+}$ -dependent gliding motility that was  
343 enhanced by incubation in extracellular  $\text{Ca}^{2+}$  in combination with glucose, demonstrating that they express a  
344 conserved mechanism for  $\text{Ca}^{2+}$  mediated motility, albeit damped by reduced stored  $\text{Ca}^{2+}$  and diminished  
345 energy levels. The damped  $\text{Ca}^{2+}$  signaling responses of bradyzoites reflect adaptations that are well suited to  
346 the long-term intracellular lifestyle of these chronic stages. As well, bradyzoites retain the potential to rapidly  
347 become motile once provided with sources of energy and calcium, demonstrating remarkable physiological  
348 flexibility that favors transmission.

349 Egress is a crucial step in the lytic cycle of apicomplexan parasites and this response requires the  
350 sequential steps of increase in cytoplasmic  $\text{Ca}^{2+}$ , secretion of micronemes, PV rupture, and activation of  
351 motility [56,57]. Our studies demonstrate that bradyzoites show minimal egress from in vitro differentiated  
352 cysts in response to agonists that normally trigger this response in tachyzoites (i.e.  $\text{Ca}^{2+}$  ionophores and  
353 zaprinast). We also demonstrate that bradyzoites are refractory to stimulation of microneme secretion using  
354 either an intracellular reporter monitoring the release of PLP1 based on the dispersion of FNR-mCherry from  
355 the cyst matrix, or a MIC2-GLuc reporter detecting secretion from extracellular bradyzoites. To explore the  
356 basis for these differences, we utilized a dual fluorescent reporter GCaMP6f BAG1-mCherry to monitor  
357 changes of cytosolic  $\text{Ca}^{2+}$  levels in bradyzoites. Calcium signaling was significantly damped in bradyzoites  
358 as reflected in delayed  $\text{Ca}^{2+}$  spikes and lower magnitude of cytosolic  $\text{Ca}^{2+}$  increases in response to  $\text{Ca}^{2+}$   
359 agonists. Reduced  $\text{Ca}^{2+}$  responses were also confirmed using bradyzoites naturally formed in C2C12 skeletal  
360 muscle cells and ex vivo cysts isolated from chronically infected mice, indicating that the damped responses  
361 are not simply a consequence of alkaline pH stress during bradyzoites development in vitro. Additionally, we  
362 observed similar damped responses from extracellular bradyzoites, indicating that decreased responses are  
363 not simply due to reduced permeability of intact cysts to agonists. To confirm these results, we also utilized  
364 Fluo-8/AM to monitor intracellular  $\text{Ca}^{2+}$  stores of bradyzoites and observed similar damped responses.  
365 Finally, since  $\text{Ca}^{2+}$ -dependent fluorescence responses by GCaMP6f or Fluo-8 are only relative and subject to  
366 differences in protein or probe levels, we developed a ratiometric calcium reporter that contains GCaMP6f  
367 fused with self-cleavage tag P2A linked mTagBFP2 under the control of the same promoter. Ratiometric  
368 measurements of the GCaMP6f signal compared to the  $\text{Ca}^{2+}$  insensitive indicator mTagBFP2, determined that  
369 bradyzoites have lower resting  $\text{Ca}^{2+}$  levels and quantitatively decreased  $\text{Ca}^{2+}$  responses relative to tachyzoites  
370 in response to  $\text{Ca}^{2+}$  agonists. Collectively, these findings conclusively show that bradyzoites have reduced  $\text{Ca}^{2+}$   
371 responses whether developed in vitro or in vivo and using a variety of independent methods to assess both  
372  $\text{Ca}^{2+}$  levels and physiological responses.

373 Based on the above findings, it seems likely that bradyzoites possess different mechanisms to control  $\text{Ca}^{2+}$

374 homeostasis, including differences in expression of  $\text{Ca}^{2+}$  channels and  $\text{Ca}^{2+}$  pumps relative to tachyzoites.  
375 These differences would impact  $\text{Ca}^{2+}$  storage pools, affecting cytosolic  $\text{Ca}^{2+}$  and signaling. For example, our  
376 findings indicate that bradyzoites show reduced responses to ionomycin and thapsigargin, which release  $\text{Ca}^{2+}$   
377 from the ER, and in response to  $\text{NH}_4\text{Cl}$ , which releases  $\text{Ca}^{2+}$  from acidocalcisomes and likely other acidic  
378 stores [35,58]. Consistent with these dampened responses, bradyzoites showed significantly reduced  
379 expression of the  $\text{Ca}^{2+}$ -ATPases TgSERCA [34] and TgA1 [36], which are involved in transporting cytosolic  
380  $\text{Ca}^{2+}$  into the ER and acidocalcisome, respectively. They also showed reduced expression of TgA2, the  $\text{Ca}^{2+}/\text{H}^+$   
381 exchanger and the recently described TRPPL-2 [53], which is a transient receptor potential (TRP) channel key  
382 for cytosolic  $\text{Ca}^{2+}$  influx through the plasma and ER membranes. The reduced expression of these genes is  
383 also supported by prior data on stage-specific transcriptional differences (<http://Toxodb.org>). Additionally, it is  
384 possible that the reduced levels of  $\text{Ca}^{2+}$  in bradyzoites reflect limitations on the availability of  $\text{Ca}^{2+}$  from the  
385 host cell, since prior studies have shown that tachyzoites acquire their intracellular  $\text{Ca}^{2+}$  from this source [37].  
386 Further studies will be needed to decipher the contribution of these various mechanism to altered calcium  
387 homeostasis and signaling in bradyzoites.

388       Bradyzoites are surrounded by a cyst wall that is comprised of an outer thin compact layer and an inner  
389 sponge-like layer that faces the cyst matrix [59]. The cyst wall is enriched in dense granule proteins [60],  
390 stage-specific glycoproteins such as CST1 [61,62], and partially characterized carbohydrates [63]. This  
391 architecture may create a barrier to egress since bradyzoites were able to activate motility but not to efficiently  
392 emerge from intact cysts. We utilized trypsin to digest the cyst wall, mimicking the cyst rupture observed in  
393 chronically infected mice or following oral ingestion and exposure to pepsin [43,64]. Notably, proteolytic  
394 release did not result in immediate changes in  $\text{Ca}^{2+}$  nor motility in the parasite, suggesting that cyst wall  
395 degradation does not trigger a process akin to egress in tachyzoites. Rather, when artificially released in this  
396 manner, a subset of bradyzoites spontaneously underwent gliding motility associated with  $\text{Ca}^{2+}$  oscillations  
397 that were similar to those previously described for tachyzoites [39]. When incubated with extracellular  $\text{Ca}^{2+}$ ,  
398 the percentage of motile bradyzoites increased dramatically, suggesting that  $\text{Ca}^{2+}$  entry stimulates motility,  
399 similar to tachyzoites [14,41]. Unlike a previous report showing that tachyzoites contain sufficient calcium  
400 stores and energy levels to be independent of external carbon sources during the first hr after liberation [65],  
401 we observed that bradyzoites require an external source of carbon to regain  $\text{Ca}^{2+}$  stores and ATP levels.  
402 Similar to previous findings that *T. gondii* tachyzoites can support motility either from glucose through  
403 glycolysis or from glutamine that feeds into the TCA cycle [66,67], we observed that either carbon source was  
404 capable of synergizing with  $\text{Ca}^{2+}$  to restore bradyzoite motility, although inhibitor studies indicate that  
405 oxidative phosphorylation is required to restore optimal energy levels. Consistent with this prediction, we  
406 observed that bradyzoites have intrinsically low ATP/ADP ratios but that they recovered substantially when  
407 incubated extracellularly for 1 hr in  $\text{Ca}^{2+}$  and glucose. Hence, reduced expression of  $\text{Ca}^{2+}$  channels that allow

408 influx into the cytosol and reduced expression of  $\text{Ca}^{2+}$  pumps that fill intracellular stores would result in a  
409 general reduction of stored  $\text{Ca}^{2+}$ . Reduced ER  $\text{Ca}^{2+}$  could impact mitochondrial  $\text{Ca}^{2+}$ , since it has been  
410 shown in mammalian cells that  $\text{Ca}^{2+}$  can be transferred directly (through membrane contact sites) from the ER  
411 to the mitochondria [68,69], which is essential for oxidative phosphorylation and ATP production. Ultimately,  
412 reduced ER  $\text{Ca}^{2+}$  may be responsible for altering energy metabolism and inducing the quiescent state in *T.*  
413 *gondii* bradyzoites. Collectively, these findings indicate that bradyzoites are characterized by both low  
414 calcium stores and low ATP levels, but that they respond rapidly to changes in the extracellular environment to  
415 restore both energy levels and  $\text{Ca}^{2+}$  signaling systems needed for motility. Stimulation of  $\text{Ca}^{2+}$  signaling is also  
416 important in breaking dormancy [70] and pollen germination in plants [71], and initiation of the cell cycle in  
417 animal cells [72], demonstrating the important role played by  $\text{Ca}^{2+}$  signaling in reactivation.

418 Reduced  $\text{Ca}^{2+}$  storage, damped  $\text{Ca}^{2+}$  signaling, and a lower energy state may reflect the long-term  
419 sessile nature of the intracellular cyst, which prolong chronic infection. The mechanisms inducing cyst wall  
420 turnover in vivo are unclear, although host cell macrophages may contribute to this process as they secrete  
421 chitinase that can lyse cysts in vitro [73]. Additionally, cyst wall turnover may be controlled by release of  
422 parasite hydrolases as suggested by the presence of GRA56, which is predicted to belong to the melibiase  
423 family of polysaccharide degrading enzymes, on the cyst wall [74]. Our in vitro studies suggest that once the  
424 cyst wall is ruptured, bradyzoites respond to higher levels of  $\text{Ca}^{2+}$  and glucose in the extracellular environment  
425 to regain motility needed for subsequent cell invasion. Emergence of bradyzoites from tissue cysts that rupture  
426 in muscle or brain, or in tissue following oral ingestion, are likely to provide an environment to recharge  
427 bradyzoites. Consistent with this idea, previous in vitro studies have shown that similar motile bradyzoites  
428 released from ruptured cysts have the ability to re-invade new host cells, establishing new cysts without an  
429 intermediate growth stage as tachyzoites [75]. Hence, the rapid metabolic recovery of otherwise quiescent  
430 bradyzoites may be important for the maintenance of chronic infection within a single host and to assure  
431 robust cellular invasion upon transmission to the next host.

432

### 433 Materials and Methods

#### 434 Cell culture

435 *Toxoplasma gondii* tachyzoites were passaged in confluent monolayers of human foreskin fibroblasts (HFFs)  
436 obtained from the Boothroyd laboratory at Stanford University. The ME49  $\Delta hxpprt::Fluc$  type II strain of *T.*  
437 *gondii* [76] was used as a parental strain for genetic modification. Tachyzoites were cultured in Dulbecco's  
438 modified Eagle's medium (DMEM; Life Technologies) pH 7.4, supplemented with 10% fetal bovine serum  
439 (FBS), penicillin, and streptomycin (Life Technologies) at 37°C in 5%  $\text{CO}_2$ . For in vitro induction of  
440 bradyzoites, parasites were cultured in alkaline medium in ambient  $\text{CO}_2$  as described previously [77]. In brief,  
441 infected HFF monolayers were switched to RPMI 1640 medium (MP Biomedicals) buffered to pH 8.2 with  
442 HEPES and supplemented with 5% FBS and cultured at 37°C in ambient  $\text{CO}_2$ , during which time the alkaline  
443 medium was changed every 2 days. For spontaneous induction of bradyzoites, C2C12 muscle myoblast cells

444 (ATCC® CRL-1772™) were maintained in DMEM supplemented with 20% FBS. C2C12 myoblast  
445 differentiation and myotube formation were induced in DMEM containing 2% horse serum (Biochrom) by  
446 cultivation at 37°C in 5% CO<sub>2</sub> for 5 days. Tachyzoites were inoculated into the differentiated muscle cells and  
447 cultured for another 7 days to induce bradyzoite formation, during which time the induction medium was  
448 changed every 2 days. For harvesting bradyzoites, infected monolayers were scraped into intracellular (IC)  
449 buffer (142 mM KCl, 5 mM NaCl, 1 mM MgCl<sub>2</sub>, 5.6 mM D-glucose, 2 mM EGTA, 25 mM HEPES, pH 7.4)  
450 and released from cells by serially passing through 18g, 20g and 25g needles, followed by centrifugation  
451 (150g, 4°C) for 10 min. The pellet containing cysts was resuspended in IC buffer. Bradyzoites were liberated  
452 from cysts by digestion with 0.25 mg/ml trypsin at room temperature for 5 min, followed by centrifugation  
453 (150g, 4°C) for 10 min. The supernatant containing liberated bradyzoites was further centrifuged (400g, 4°C)  
454 for 10 min. The pellet containing purified bradyzoites was resuspended in extracellular (EC) buffer (5 mM  
455 KCl, 142 mM NaCl, 1 mM MgCl<sub>2</sub>, 5.6 mM D-glucose, 25 mM HEPES, pH 7.4) with (1.8 mM Ca<sup>2+</sup>) or  
456 without CaCl<sub>2</sub>, as indicated for different assays and in the legends.

#### 457 **Reagents and antibodies**

458 A23187, zaprinast, ionomycin, thapsigargin, NH<sub>4</sub>Cl, Fluorescein isothiocyanate-conjugated *Dolichos biflorus*  
459 agglutinin (DBA), and BAPTA-AM were obtained from Sigma. Fluo-8 AM was obtained from Abcam.  
460 SYTOX™ Red Dead Cell Stain was obtained from Thermal Fisher. The compounds 3-MB-PP1 [51] and  
461 Compound 1 [42] were obtained as described previously. Trypsin and L-glutamine were purchased from MP  
462 Biomedicals. Adenosine 5'-triphosphate (ATP) disodium salt, adenosine 5' -diphosphate (ADP) sodium salt,  
463 adenosine 5' -monophosphate (AMP) disodium salt, oligomycin A and 2-deoxy-D-glucose were purchased  
464 from Sigma. Primary antibodies include mouse mAb DG52 anti-SAG1 (provided by John Boothroyd), mouse  
465 mAb 6D10 anti-MIC2 [78], rabbit anti-GRA7 [79], mouse mAb 8.25.8 anti-BAG1 (obtained from Louis  
466 Wiess), rabbit anti-BAG1 (obtained from Louis Wiess), mouse anti-c-myc (mAb 9E10, Life Technologies),  
467 mouse anti-acetylated Tubulin (mAb 6-11B-1, Sigma), rat anti-mCherry (mAb 16D7, Life Technologies),  
468 rabbit-anti SRS9 (obtained from John Boothroyd), rabbit anti-tRFP (Axxora), mouse anti-6XHis (mAbHIS.H8,  
469 Life Technologies). Secondary antibodies for immunofluorescence assays include goat anti-mouse IgG  
470 conjugated to Alexa Fluor-488, goat anti-rabbit IgG conjugated to Alexa Fluor-488, anti-mouse IgG  
471 conjugated to Alexa Fluor-568, goat anti-rat IgG conjugated to Alexa Fluor-568, goat anti-mouse IgG  
472 conjugated to Alexa Fluor-594 (Life Technologies). For Western blotting, secondary antibodies consisted of  
473 goat anti-mouse IgG, goat anti-rabbit IgG, or goat anti-rat IgG conjugated to LiCor C800 or C680 IR-dyes and  
474 detected with an Odyssey Infrared Imaging System (LI-COR Biotechnology).

#### 475 **Generation of stable transgenic parasite lines**

##### 476 *Dual calcium and bradyzoite reporter strain: BAG1-mCherry GCaMP6f*

477 A dual reporter strain designed to detect bradyzoite conversion and calcium fluctuation was generated in the  
478 ME49  $\Delta$ hxgprt::Fluc strain [76]. We generated a plasmid named pNJ-26 that contains mCherry driven by the  
479 BAG1 promoter, the genetically encoded calcium indicator GCaMP6f under the control of Tubulin1 promoter,  
480 and selection marker cassette SAG1 promoter driving CAT. ME49  $\Delta$ hxgprt::Fluc tachyzoites were transfected  
481 with 20 µg pNJ-26 plasmid and selected with 20 µM chloramphenicol. Clones containing randomly integrated  
482 transgenes were confirmed by diagnostic PCR and by IFA staining. Primers are shown in Supplementary table

483 1.

484 *Bradyzoite reporter strain: BAG1-EGFP and BAG1-mCherry*

485 The BAG1 promoter and the mCherry open reading frame (ORF) were independently PCR amplified from  
486 pNJ-26 and the EGFP ORF was amplified from pSAG1::CAS9-U6::sgUPRT respectively. The BAG1 promoter  
487 fragment and EGFP ORF or mCherry (ORF) were cloned by NEBuilder HiFi DNA Assembly Cloning Kit  
488 (NEB, E5520S) into the vector backbone that was produced by double enzymatic digestion of  
489 pTUB1::YFP-mAID-3HA, DHFR-TS::HXGPRT using KpnI and NdeI. ME49  $\Delta$ hxgprt::Fluc tachyzoites were  
490 transfected with 20  $\mu$ g pBAG1::EGFP, DHFFR-TS::HXGPRT or pBAG1::mCherry, DHFFR-TS::HXGPRT and  
491 selected with mycophenolic acid (MPA) (25  $\mu$ g/ml) and 6-xanthine (6Xa) (50  $\mu$ g/ml). Single cell clones  
492 containing randomly integrated transgenes were confirmed by diagnostic PCR and by IFA staining. Primers  
493 are shown in Supplementary table 1.

494 *MIC2 secretion reporter BAG1-mCherry MIC2-GLuc*

495 The bradyzoite reporter line BAG1-mCherry was transfected with 20  $\mu$ g of the previously described  
496 pMIC2::GLuc-myc, DHFR-TS plasmid [42] and selected with 3  $\mu$ M pyrimethamine (PYR). Single cell clones  
497 containing randomly integrated transgenes were confirmed by diagnostic PCR and by IFA staining.

498 *FNR-mCherry leakage reporter BAG1-EGFP FNR-mCherry*

499 The bradyzoite reporter line BAG1-EGFP was transfected with 20  $\mu$ g pTUB1::FNR-mCherry, CAT (provided  
500 by the Carruthers lab) and selected with 20  $\mu$ M chloramphenicol. Single cell clones containing randomly  
501 integrated transgenes were confirmed by diagnostic PCR and by IFA staining.

502 *Ratiometric reporter BAG1-mCherry GCaMP6f-P2A-mTagBFP2*

503 The ratiometric reporter strain was generated using targeted insertion with CRISPR/Cas9 using previously  
504 described methods [80] to add the blue fluorescent protein (BFP) downstream of the GCaMP6f protein in the  
505 strain BAG1-mCherry GCaMP6f. In brief, a single guide RNA (sgRNA) targeting the DHFR 3'UTR  
506 following the GCaMP6f coding sequence was generated in the plasmid pSAG1::CAS9-U6::sgUPRT [81]. The  
507 P2A-mTagBFP2 tagging plasmid was constructed by cloning a synthetic sequence containing a slit peptide  
508 (P2A) together with the blue fluorescent reporter mTagBFP2 (P2A-mTagBFP2) into the  
509 pTUB1::YFP-mAID-3HA, DHFR-TS::HXGPRT backbone by NEBuilder HiFi DNA Assembly Cloning Kit  
510 (NEB, E5520S) after double enzymatic digestion of KpnI and NdeI. Following this step, the SAG1 3'UTR  
511 was amplified from pNJ-26 and cloned into the tagging plasmid to replace DHFR 3'UTR by Gibson assembly  
512 (NEB, E5520S). BAG1-mCherry GCaMP6f reporter tachyzoites were co-transfected with 10  $\mu$ g of  
513 pSAG1::CAS9-U6::sgDHFR 3'UTR and 2  $\mu$ g of PCR amplified P2A-mTagBFP2-HXGPRT flanked with 40  
514 bp homology regions, as described previously [26]. Stable transfectants were selected with 25  $\mu$ g/ml MPA and  
515 50  $\mu$ g/ml 6Xa. Single cell clones containing targeted integrated transgenes were confirmed by diagnostic PCR  
516 and by IFA staining. Primers are shown in Supplementary Table S1.

517 **Time-lapse imaging of fluorescent reporter strains**

518 For time-lapse microscopy, extracellular parasites were added to glass-bottom culture dishes (MatTek), or  
519 intracellular parasites were grown in host cells attached glass-bottom culture dishes. Alternating phase and  
520 fluorescent images (at different intervals specified in the legends) were collected on a Zeiss AxioObserver Z1  
521 (Carl Zeiss, Inc.) equipped with an ORCA-ER digital camera (Hamamatsu Photonics) and a 20x EC

522 Plan-Neofluar objective (N.A. 0.50), 37°C heating unit, and LED illumination for blue, green, red and far-red  
523 wavelengths. Spinning disk images were acquired with a 100x oil Plan-Apochromat (N.A. 1.46) objective  
524 using illumination from 488 nm and 561 nm solid state lasers (Zeiss) and Evolve 512 Delta EMCCD cameras  
525 (Photometrics) attached to the same Zeiss AxioObserver Z1 microscope. Images were acquired and analyzed  
526 using Zen software 2.6 blue edition (Zeiss). Fluorescent intensity changes ( $F/F_0$ ) vs. time were plotted with  
527 GraphPad Prism version 6 (GraphPad Software, Inc.).

528 **Indirect immunofluorescence assay (IFA)**

529 Parasites grown in HFF monolayers on glass coverslips were fixed in 4% (v/v) formaldehyde in PBS for 10  
530 min, and permeabilized by 0.25% (v/v) Triton X-100 in PBS for 20 min, and blocked in 3% bovine serum  
531 albumin (BSA) in PBS. Monolayers were incubated with different primary antibodies and visualized with  
532 secondary antibodies conjugated to Alexa Fluors. Coverslips were sealed onto slides using ProLong™ Gold  
533 Antifade containing DAPI (Thermo Fisher Scientific). Images were captured using a 63x oil Plan-Apochromat  
534 lens (N.A. 1.4) on an Axioskop2 MOT Plus Wide Field Fluorescence Microscope (Carl Zeiss, Inc). Scale bars  
535 and linear adjustments were made to images using Axiovision LE64 software (Carl Zeiss, Inc.).

536 **Western Blotting**

537 Samples were prepared in 5X Laemmli buffer containing 100 mM dithiothreitol, boiled for 5 min, separated  
538 on polyacrylamide gels by SDS-PAGE, and transferred to nitrocellulose membrane. Membranes were blocked  
539 with 5% nonfat milk, probed with primary antibodies diluted in blocking buffer. Membranes were washed  
540 with PBS + 0.1% Tween 20, then incubated with goat IR dye-conjugated secondary antibodies (LI-COR  
541 Biosciences) in blocking buffer. Membranes were washed several times before scanning on a LiCor Odyssey  
542 imaging system (LI-COR Biosciences).

543 **Fluo-8 AM calcium monitoring**

544 Freshly harvested parasites were loaded with 500 nM Fluo-8 AM for 10 min at room temperature, followed by  
545 centrifugation at 400 g for 5 min and washing in EC buffer without  $\text{Ca}^{2+}$ . Parasites were resuspended in EC  
546 buffer without  $\text{Ca}^{2+}$  and added directly to glass-bottom culture dishes. After addition of agonists, time-lapse  
547 images were recorded and analyzed as described above.

548 **Egress assay**

549 Infected cells were treated with 2  $\mu\text{M}$  A23187 or 500  $\mu\text{M}$  zaprinast for 15 min at 37°C. Following incubation,  
550 samples were stained by IFA using antibodies against SAG1 (mouse), GRA7 (rabbit), FITC-conjugated DBA  
551 or BAG1(rabbit) and followed by secondary antibodies conjugated to Alexa Fluors. Samples were examined  
552 by fluorescence microscopy and the percentages of egressed or released parasites per vacuole or cyst were  
553 determined at least for 20 vacuoles or cysts per experiment. The maximum egress distance of parasites from  
554 vacuole or cysts were measured from scanned tiff images in imageJ.

555 **Flow cytometry**

556 ME49 BAG1-mCherry MIC2-GLuc reporter bradyzoites were induced for 7 days at pH 8.2, harvested in IC  
557 buffer as described above, and passed through 5  $\mu\text{m}$  polycarbonate membrane filter. ME49  $\Delta hxpprt::Fluc$   
558 tachyzoites, cultured and harvested as indicated above, were used for gating. Approximately  $1 \times 10^6$  parasites  
559 from each sample (ME49 BAG1-mCherry MIC2-GLuc reporter tachyzoites and ME49 BAG1-mCherry  
560 MIC2-GLuc reporter bradyzoites) were sorted on Sony SH800S Cell Sorter directly into 500  $\mu\text{l}$  IC buffer

561 followed by centrifugation. Flow cytometry data were processed using FlowJo version 10 (FLOWJO, LLC).

562 **Collection of excretory-secretory antigens (ESA) and *Gaussia Luciferase* Assay**

563 FACS sorted MIC2-GLuc reporter tachyzoites and bradyzoites were suspended with EC buffer and incubated  
564 with different agonists at 37°C for 10 min. ESA was collected by centrifugation and mixed with Pierce™  
565 *Gaussia Luciferase* Glow Assay Kit reagent (Thermo Scientific™) and luminescence was detected using a  
566 Cytation 3 Cell Imaging Multimode Imager (BioTek Instruments, Inc.). Buffer control values were subtracted  
567 from their corresponding sample values to correct for background.

568 **Real-time PCR**

569 RNA was extracted from ME49  $\Delta hxpprt::Fluc$  tachyzoites and bradyzoites induced for 7 days at pH 8.2 using  
570 RNeasy Mini Kit (Qiagen) combined with QIAshredder (Qiagen) followed by DNA Removal using  
571 DNA-free™ DNA Removal Kit (Thermo Fisher) and subsequent reverse transcription using High-Capacity  
572 cDNA Reverse Transcription Kit (Thermo Fisher). Quantitative real-time PCR was performed on Applied  
573 Biosystems QuantStudio 3 Real-Time PCR System (Thermo Fisher) using SYBR® Green JumpStart™ Taq  
574 ReadyMix™ (Sigma) with primers shown in Supplementary table 1. Mean fold changes from two  
575 independent experiments were calculated from  $\Delta\Delta$  Ct values using actin1 transcript as housekeeping gene, as  
576 described previously [82].

577 **Gliding trail assay**

578 Coverslips were precoated by incubation in 50% fetal bovine serum diluted in PBS for 1 h at 37°C followed  
579 by rinsing in PBS. Freshly harvested tachyzoites or bradyzoites were resuspended in EC buffer, treated with  
580 DMSO (0.1%, v/v), or inhibitors (in 0.1% DMSO, v/v) and then added to pre-coated glass coverslips and  
581 incubated at 37°C for 15 min. Coverslips were fixed in 2.5% formalin in PBS for 10 min and the surface  
582 proteins were detected by IFA as above described using anti-SAG1 and anti-SRS9 antibodies as stage-specific  
583 markers for tachyzoites and bradyzoites, respectively. Gliding trails were captured by IFA microscopy as  
584 described above and the frequency of trails measured from tiff images using ImageJ.

585 **Gliding motility assay based on time-lapse video microscopy**

586 BAG1-mCherry parasites were induced to form bradyzoites by culture at pH 8.2 in RPMI 1640 medium under  
587 ambient air (low CO<sub>2</sub>) for 7 days followed by scraping into IC buffer (without glucose) and repeated passage  
588 through a 23g needle. Intact, but extracellular cysts, were pellet by centrifugation at 150 g for 10 min and  
589 resuspended in IC buffer without glucose. During purification, all procedures were performed at 16°C.  
590 MatTek 25 mm dishes glass bottom dishes (coverslip dishes) were pre-coated with 2 ml 50% FBS at 4°C  
591 overnight and rinsed twice using PBS prior to use. Purified cysts were added to the precoated coverslip dishes  
592 in IC buffer containing 0.25mg/ml trypsin and incubated for 10 min at 16°C. The medium was removed and 2  
593 ml EC buffer  $\pm$  1.8 mM Ca<sup>2+</sup> and/or  $\pm$  5.6 mM glucose was added and incubated for 10 min or 1 hr at 16°C.  
594 Prior to imaging, the coverslip dishes were heated to 37 °C using a Heating Unit XL S (Zeiss) attached to the  
595 Zeiss AxioObserver Z1 (Carl Zeiss, Inc.). Images were collected under bright field illumination using a 40x  
596 C-Apochromat water immersion objective (N.A. 1.20), and ORCA-ER digital camera (Hamamatsu Photonics  
597 at 1 sec intervals for 5 min per field. The percentage of BAG1-mCherry positive bradyzoites displaying  
598 different types of gliding motility was calculate from 6 movies per sample. Images were imported into NIH  
599 ImageJ with a Cell Counter plug-in for quantification of the types of motility based on visual inspection.

600 **High-performance liquid chromatography UV (HPLC-UV) analysis of ATP, ADP and AMP levels in**  
601 **bradyzoites** BAG1-mCherry parasites were induced to form bradyzoites by culture at pH 8.2 in RPMI 1640  
602 medium under ambient air (low CO<sub>2</sub>) for 7 days followed by scraping into ice-cold PBS containing 0.05%  
603 BSA. Cysts were released from host cells by repeated passage through a 23 g needle and collected by  
604 centrifugation at 150 g for 10 min. To purify bradyzoites, cysts were resuspended in 1 ml EC buffer without  
605 calcium or glucose but containing 10  $\mu$ l biotinylated DBA (Vector laboratories) and 100  $\mu$ l Pierce Streptavidin  
606 Magnetic Beads (Thermo Fisher) and incubated for 1 hr at 4°C. The beads and absorbed cysts were collected  
607 using a magnetic stand and resuspended in 1 ml EC buffer without calcium or glucose but containing 0.25  
608 mg/ml trypsin and incubated for 10 min at 4°C. The supernatant containing released parasites was separated  
609 from the beads and retained. To remove any residual tachyzoites in the supernatant, 5  $\mu$ l of mAb DG52  
610 pre-coupled to 100  $\mu$ l Dynabeads™ Protein G (Thermo Fisher) was added to the supernatant and incubated  
611 for 1 hr at 4°C. The supernatant was separated from the beads, bradyzoites centrifuged at 600 g, 4°C for 10  
612 min, and resuspended in 1 ml EC buffer containing 1.8 mM Ca<sup>2+</sup> and 5.6 mM glucose for 10 min or 1 hr at  
613 room temperature. Following incubation, the bradyzoites were pelleted at 600 g, 4°C for 10 mi and stored at  
614 -80°C until analysis.

615 A previously described method for extraction of ATP, ADP and AMP [83] was adapted for use here. In  
616 brief, 95  $\mu$ l of extraction buffer (0.3 M perchloric acid (HClO<sub>4</sub>), 1 mM ethylenediaminetetraacetic acid  
617 disodium salt (Na<sub>2</sub>EDTA), pH 8.0) was used to resuspend cell pellets and incubated for 5 min at room  
618 temperature. Extraction was stopped by addition of 17  $\mu$ l of neutralization buffer (2 M potassium hydroxide)  
619 to the samples followed by mixing. Samples were centrifuged at 14,000 g for 10 min at 4°C and the  
620 supernatant was transferred to a new tube for HPLC analysis. Analysis was performed using an HPLC system  
621 consisting of a SPD-20A UV/VIS detector (Shimadzu) equipped with SIL-20A autosampler (Shimadzu), with  
622 a Luna Omega Polar C18 column (4.6 mm internal diameter  $\times$  150 mm length, 3  $\mu$ m particle size, 100 Å pore  
623 size), and LC-20AD pump (Shimadzu). The protocol was set up as isocratic separation using a mobile phase  
624 containing 0.1 M ammonium dihydrogen phosphate (NH<sub>4</sub>H<sub>2</sub>PO<sub>4</sub>, Sigma), pH 6.0, containing 1% methanol  
625 with a flow rate of 0.8 ml/min. Injection volume was 30  $\mu$ l and peak detection was monitored at 254 nm. A  
626 series of standards containing ATP, ADP and AMP with different concentrations were used to establish  
627 retention times and standard calibration curves by calculating peak area. Samples from two independent  
628 biological replicates were analyzed using three technical replicates. The retention time and peak areas were  
629 used to calculate the corresponding concentration of each nucleotide from each sample according to the  
630 standard curve.

### 631 **Mouse infections and ex vivo cyst collection**

632 Mice were housed in an Association for Assessment and Accreditation of Laboratory Animal Care  
633 International-approved facility at Washington University School of Medicine. All animal studies were  
634 conducted in accordance with the U.S. Public Health Service Policy on Humane Care and Use of Laboratory  
635 Animals, and protocols were approved by the Institutional Animal Care and Use Committee at the School of  
636 Medicine, Washington University in St. Louis.

637 Eight-week old female CD-1 mice (Charles River) were infected with 200 ME49 BAG1-mCherry GCaMP6f

638 tachyzoites by intraperitoneal injection. After 30 days of infection, animals were sacrificed, the brain removed  
639 and homogenized and the number of brain cyst was determined by DBA staining and microscopy as  
640 previously described [77]. Eight-week old female CD-1 mice (Charles River) were infected with 5 cysts from  
641 the brain homogenate by oral gavage. Following a 30-day period these mice were euthanized, and brain  
642 homogenate was collected and added to glass bottom dishes for live imaging of tissue cysts.

643 **Statistical Analyses**

644 Statistical analyses were performed in Prism (GraphPad). Data that passed normally distribution were  
645 analyzed by one-way ANOVA or Student's t tests, while data that were not normally distributed, or contain too  
646 few samples to validate the distribution, were analyzed by Mann Whitney or Kruskal-Wallis non-parametric  
647 tests. \*,  $P < 0.05$ , \*\*,  $P < 0.01$ , \*\*\*,  $P < 0.001$ .

648

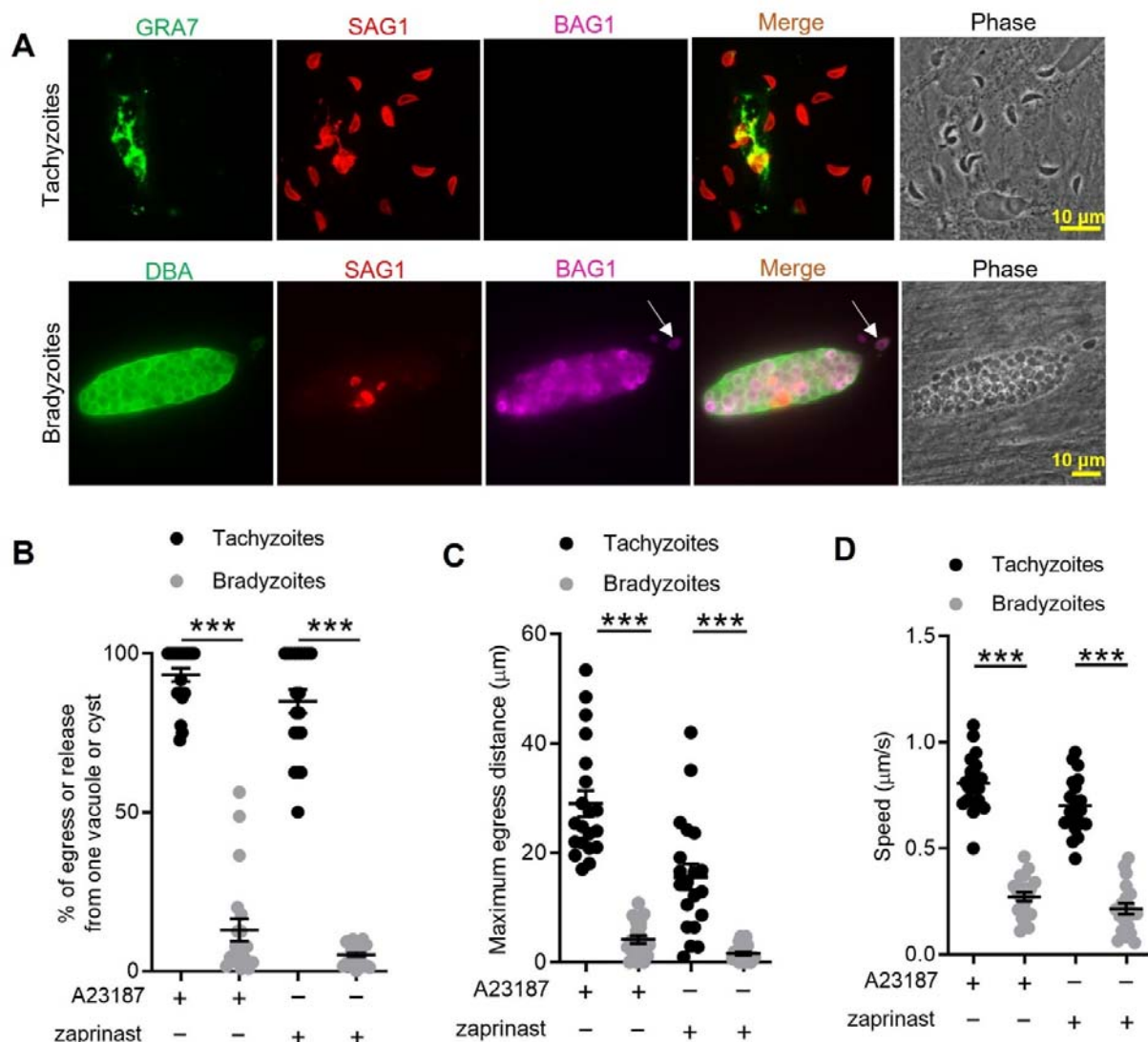
649 **Acknowledgements:** We thank Jennifer Powers Carson for technical help with the HPLC analysis which  
650 was performed in the Washington University Core Laboratory for Clinical Studies. We thank Vern Carruthers  
651 for providing plasmids, Louis Wiess and John Boothroyd for providing antibodies, members of the Sibley lab  
652 for helpful advice, Wandy Beatty, Microbiology Imaging Facility, for technical assistance with microscopy,  
653 and Jenn Barks for tissue culture support. Supported in part by a grant from the NIH (AI#034036).

654

655 **Author Contributions:** Conceived and designed the experiments: Y.F., L.D.S.; Performed the experiments: Y.F.;  
656 Analyzed the data: Y.F., S.M., L.D.S.; Provided critical reagent and experimental advice: K.M.B., N.J., S.M.;  
657 Supervised the work S.M., L.D.S.; Wrote the manuscript: Y.F., L.D.S.; Edited the manuscript, all authors.

658

659 **Disclosures:** The authors have no conflicts to disclose.



660 **Figure 1. In vitro induced bradyzoites show limited egress in response to  $\text{Ca}^{2+}$  agonists.** (A) Egress of  
661 tachyzoites and bradyzoites in response to A23187 (2  $\mu$ M) for 15 min. Anti-GRA7, anti-SAG1, and  
662 anti-BAG1 antibodies followed by secondary antibodies to Alexa conjugated fluorochromes were used to  
663 detect the parasitophorous vacuole (PV) membrane, tachyzoites, and bradyzoites, respectively. DBA  
664 (*Dolichos biflorus* agglutinin) conjugated to FITC was used to stain the cyst wall. Arrow indicates released  
665 bradyzoites. Scale bar = 10  $\mu$ m. (B) Quantitative analysis of egress in response to A23187 (2  $\mu$ M) or zaprinast  
666 (500  $\mu$ M) in extracellular buffer (EC) with  $\text{Ca}^{2+}$  for 15 min. Each data point represents the % of egressed or  
667 released parasites from one parasitophorous vacuole (PV) or cyst (n=20). Means  $\pm$  SD of two independent  
668 experiments with 20 replicates. Two-tailed Mann-Whitney test, \*\*\*P < 0.001. (C) Quantitative analysis of  
669 maximum distance egressed or released parasites moved away from the vacuole/cyst in response to A23187 (2  
670  $\mu$ M) or zaprinast (500  $\mu$ M) in EC buffer with  $\text{Ca}^{2+}$  for 15 min. Each data point represents distance travelled of  
671 one egressed tachyzoite or released bradyzoite from the original PV or cyst (n=20). Means  $\pm$  SD of two  
672 independent experiments with 20 replicates. Two-tailed Mann-Whitney test, \*\*\*P < 0.001. (D) Quantitative  
673 analysis of speed ( $\mu$ m/s) of egressed or released parasites in response to A23187 (2  $\mu$ M) or zaprinast (500  $\mu$ M)  
674 in EC buffer with calcium for 15 min by time-lapse microscopy. Mean speed was determined by time lapse  
675 recording during the first 1 min after egress or release. Each data point represents migration speed of a single  
676 parasite. Means  $\pm$  SD of two independent experiments with 20 replicates. Two-tailed Mann-Whitney test, \*\*\*P < 0.001.

677 egressed tachyzoites or released bradyzoites from original PV or cyst (n=20). Means  $\pm$  SD of two independent  
 678 experiments with 20 replicates. Two-tailed unpaired Student's t test, \*\*\* $P < 0.001$ .  
 679  
 680

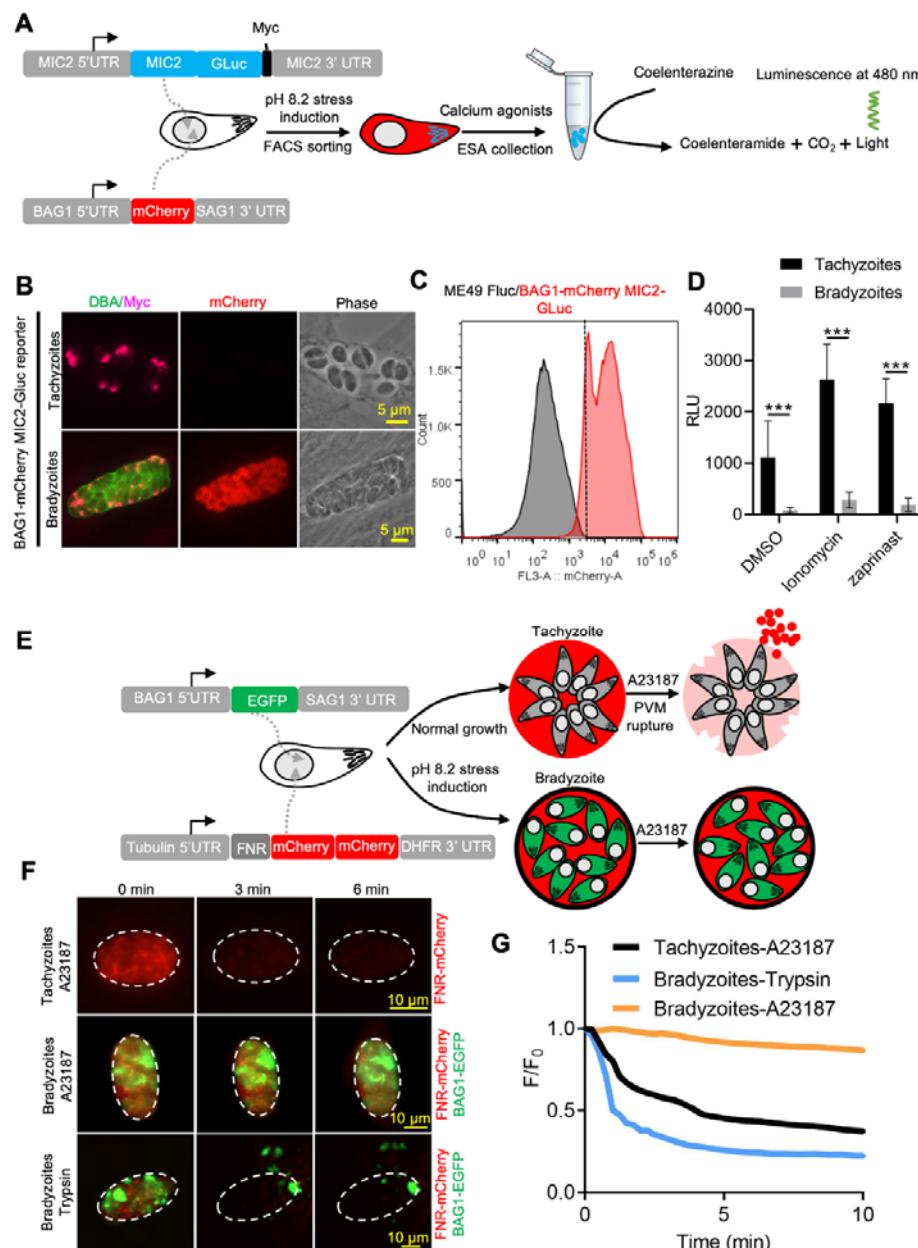


Figure 2. Ca<sup>2+</sup>

681  
 682 **dependent microneme secretion is significantly dampened in bradyzoites.** (A) Schematic of bradyzoites  
 683 MIC2 secretion assay using ME49 BAG1-mCherry MIC2-GLuc bradyzoites, differentiated in vitro by  
 684 cultivation at pH 8.2 for 7 days, based on fluorescence-activated cell sorting (FACS). (B) IFA analysis  
 685 showing localization of MIC2-Gluc in bradyzoites induced for 7 days at pH 8.2. MIC2-Gluc was stained with  
 686 anti-Myc antibody, bradyzoites were detected with anti-mCherry, followed by secondary antibodies  
 687 conjugated with Alexa Fluor dyes, and the cyst wall was stained with DBA-FITC. Bar = 5  $\mu$ m. (C)  
 688 Bradyzoites expressing BAG1-mCherry were induced for 7 days at pH 8.2, mechanically liberated from cysts  
 689 by 0.25 mg/ml trypsin for 5 min in intracellular buffer (IC buffer) and collected by FACS after gating with

690 parental ME49  $\Delta hxpprt::Fluc$  parasites. (D) ME49 BAG1-mCherry MIC2-Gluc tachyzoites or bradyzoites  
691 sorted by FACS and resuspended in EC buffer with calcium were stimulated by 0.1% DMSO, ionomycin (1  
692  $\mu\text{M}$ ) or zaprinast (500  $\mu\text{M}$ ) for 10 min at 37 °C. Release of MIC2-GLuc in ESA was determined using a  
693 *Gaussia* luciferase assay. Means  $\pm$  SEM of three independent experiments each with 3 replicates. Multiple  
694 Student's t tests, \*\*\* $P < 0.001$ . (E) Schematic illustration of the FNR-mCherry BAG1-EGFP dual  
695 fluorescence reporter and leakage of FNR-mCherry from the PV (top) or cyst matrix (bottom) following  
696 A23187-induced membrane permeabilization. (F) FNR-mCherry leakage was monitored by time-lapse  
697 imaging of FNR-mCherry after A23187 (2  $\mu\text{M}$ ) treatment. FNR-mCherry BAG1-EGFP tachyzoites cultured  
698 under normal condition for 24 hr or bradyzoites induced for 7 days at pH 8.2 were treated with A23187 (2  $\mu\text{M}$ )  
699 or 0.25 mg/ml trypsin in EC buffer with calcium for 10 min at 37°C. Dash circle indicates the region of interest  
700 (ROI) for measurement of fluorescence intensity. Bar= 10  $\mu\text{m}$ . (G) FNR-mCherry fluorescence (F) over the  
701 initial signal ( $F_0$ ) vs. time from cells treated as in F. Curves are the mean data of 3 independent vacuoles or  
702 cysts. Bradyzoites treated with DMSO group was used to assess photobleaching of mCherry (grey line).

703

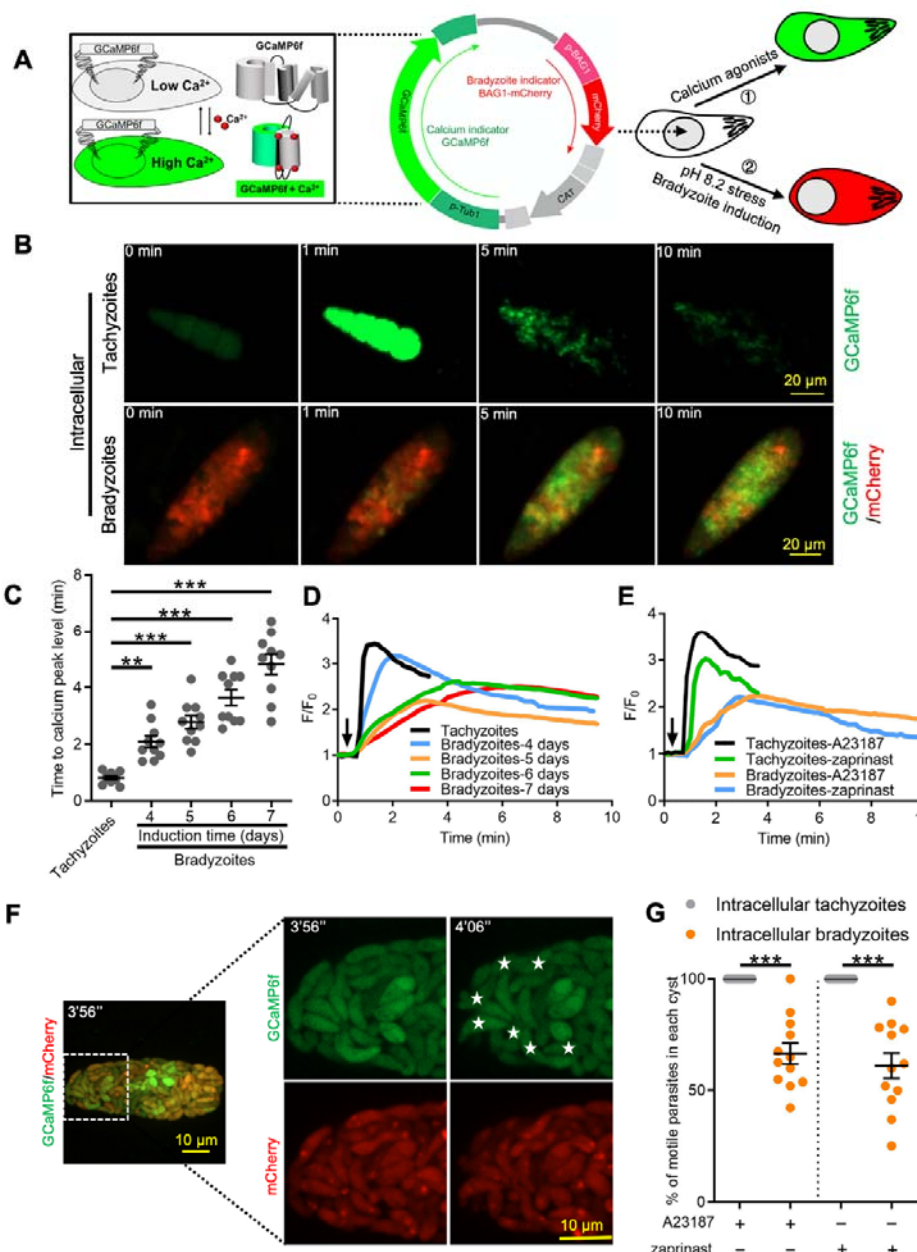


Figure 3.  $\text{Ca}^{2+}$

704

705 **signaling is dampened during in vitro bradyzoite development induced by alkaline pH.** (A) Schematic of  
 706 generation of BAG1-mCherry and GCaMP6f dual fluorescent reporter to monitor  $\text{Ca}^{2+}$  responses in  
 707 bradyzoites. (B) Time-lapse images BAG1-mCherry GCaMP6f tachyzoites cultured for 24 hr vs. bradyzoites  
 708 induced for 7 days at pH 8.2 in response to A23187 (2  $\mu\text{M}$ ) in EC buffer with  $\text{Ca}^{2+}$  for 10 min. Bar= 20  $\mu\text{m}$ .  
 709 (C) Time for reaching  $\text{Ca}^{2+}$  peak level in response to A23187 (2  $\mu\text{M}$ ) for BAG1-mCherry GCaMP6f  
 710 expressing tachyzoites and bradyzoites induced at pH 8.2. Data points of each group represent 10 cysts or  
 711 vacuoles. Means  $\pm$  SD of two independent experiments with 10 replicates each. One way ANOVA with  
 712 Dunn's multiple comparison correction test \*\*,  $P < 0.01$ , \*\*\*,  $P < 0.001$ . (D) Monitoring the relative intensity  
 713 of GCaMP fluorescence fold change ( $F/F_0$ ) vs. time for intracellular tachyzoites and in vitro induced  
 714 bradyzoites induced at pH 8.2. Cells were treated with A23187 (2  $\mu\text{M}$ ) in EC buffer without  $\text{Ca}^{2+}$  for 10 min.  
 715 Curves are the mean fluorescence intensity of 3 vacuoles or cysts. Arrow indicates time of addition of A23187.

716 (E) Monitoring the relative intensity of GCaMP fluorescence vs. time for intracellular tachyzoites and in vitro  
717 induced bradyzoites (5 days at pH 8.2). Cells were treated with A23187 (2  $\mu$ M) or zaprinast (500  $\mu$ M) in EC  
718 buffer with  $\text{Ca}^{2+}$ . Arrow indicates time of addition of agonists. Curves represent the mean data of 3  
719 independent cysts or vacuoles. (F) Live time-lapse imaging of BAG1-mCherry GCaMP6f bradyzoites induced  
720 for 7 days at pH 8.2 in response to A23187 (2  $\mu$ M) in EC buffer with calcium. Cells were imaged by spinning  
721 disc confocal microscopy after reaching calcium peak levels (left panel). Right panel showed its  
722 corresponding zoomed-in images. The interval between two continuous images is 10 s, white asterisks in the  
723 latter image (4'06'') indicate motile bradyzoites by comparison with the former image (3'56''). Bar= 10  $\mu$ m.  
724 (G) Motility of parasites within PVs or cysts was analyzed by time-lapse spinning disc confocal microscopy  
725 and tracking of individual parasites for 5 min after reaching  $\text{Ca}^{2+}$  peak levels in response to A23187 (2  $\mu$ M) or  
726 zaprinast (500  $\mu$ M) in EC buffer with calcium. Each data point represents parasites from one vacuole or cyst  
727 (n=10). Data come from two independent experiments. Two-tailed Mann-Whitney test, \*\*\* $P < 0.001$ . Lines  
728 and error bars represent means  $\pm$  SD of two independent experiments with 10 replicates each.

729

730

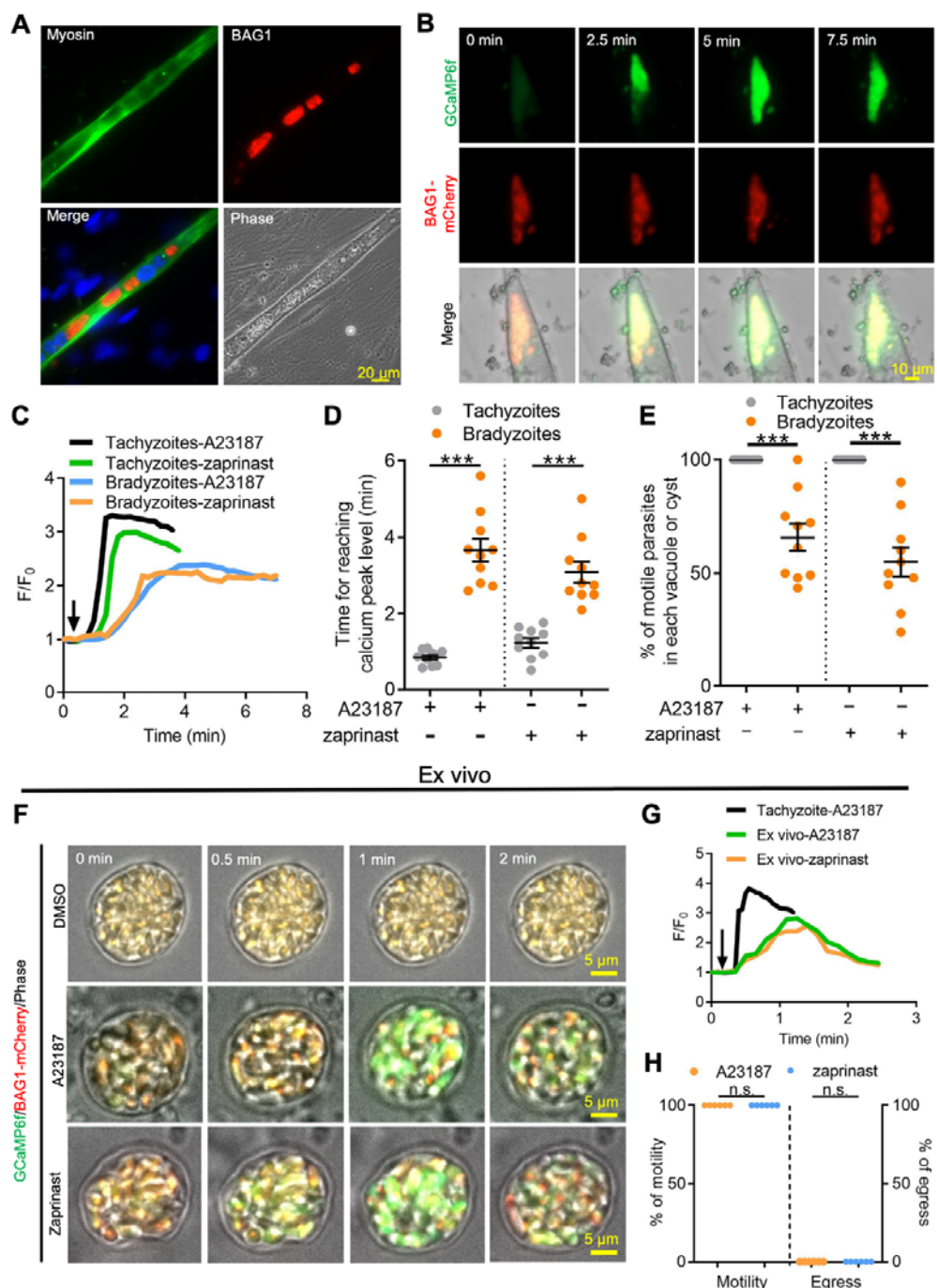


Figure 4.  $\text{Ca}^{2+}$

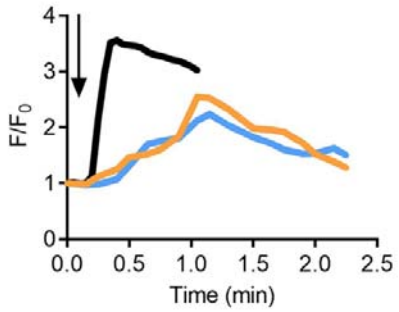
731

732 **signaling is dampened in in vitro bradyzoites from spontaneously formed cysts in C2C12 muscle cells**  
 733 **and cysts isolated from chronically infected mice.** (A) Microscopy based assay for detection of bradyzoites  
 734 naturally formed after 7 days culture of the BAG1-mCherry GCaMP6f expressing dual reporter strain in  
 735 differentiated C2C12 muscle cells. Anti-myosin antibody was used to confirm the differentiation of C2C12  
 736 cells while BAG1 was used to detect bradyzoites followed by secondary antibodies conjugated with Alexa  
 737 Fluor dyes. Bar = 20  $\mu$ m. (B) Time-lapse recording of GCaMP6f fluorescence intensity from cysts of the  
 738 BAG1-mCherry GCaMP6f strain naturally formed after 7 days culture in C2C12 cells. Cells were treated with  
 739 A23187 (2  $\mu$ M) in EC buffer with  $\text{Ca}^{2+}$ . Bar = 10  $\mu$ m. (C) GCaMP6f fluorescence intensity changes vs. time  
 740 from tachyzoites cultured in undifferentiated myoblasts or cysts naturally formed after 10 days in

741 differentiated C2C12 cells in response to A23187 (2  $\mu$ M) or zaprinast (500  $\mu$ M) in EC buffer with calcium.  
742 Curves represent mean data of 3 independent cysts or vacuoles. (D) Time for reaching  $\text{Ca}^{2+}$  peak levels in  
743 tachyzoites cultured in undifferentiated myoblasts and bradyzoites formed after 10 days culturing in C2C12  
744 cells. Cells were treated with A23187 (2  $\mu$ M) or zaprinast (500  $\mu$ M) in EC buffer with calcium for 10 min.  
745 Data points of each group come from 10 cysts or vacuoles of two independent experiments. Two-tailed  
746 unpaired Student's t test, \*\*\* $P < 0.001$ . Lines represent means  $\pm$  SD of two independent experiments with 10  
747 replicates each. (E) Motility of parasites analyzed by time-lapse spinning disc confocal microscopy and  
748 tracking of individual parasites for 5 min after reaching calcium peak levels in response to A23187 (2  $\mu$ M) or  
749 zaprinast (500  $\mu$ M) in EC buffer with calcium. Lines represent means  $\pm$  SD of two independent experiments  
750 with 10 replicates each. Two-tailed Mann-Whitney t test, \*\*\* $P < 0.001$ . (F) Monitoring of GCaMP  
751 fluorescence in response to 0.1% DMSO, A23187 (2  $\mu$ M) or zaprinast (500  $\mu$ M) in EC buffer with  $\text{Ca}^{2+}$  in ex  
752 vivo cysts isolated from the brains of mice infected with BAG1-mCherry GCaMP6f reporter parasites. Cysts  
753 were harvested at 30 days post infection. Bar = 5  $\mu$ m. (G) GCaMP6f fluorescence intensity changes vs. time  
754 within BAG1-mCherry GCaMP6f ex vivo cysts in response to A23187 (2  $\mu$ M) or zaprinast (500  $\mu$ M) in EC  
755 buffer with calcium. Curves are the mean data of 3 independent cysts. (H) Quantitative analysis of motility  
756 and egress by bradyzoites from ex vivo cysts isolated from CD-1 mice brain tissues at 30 days post-infection.  
757 Motility was analyzed by time-lapse microscopy and tracking of individual parasites using time points similar  
758 to D, E above. Each data point represents percentage of motile or egressed parasites from one cyst (n=5).  
759 Significance was determined by two-tailed Student's t-test, n.s., not significant.

760

- Extracellular tachyzoites-A23187
- Extracellular in vitro cyst-A23187
- Extracellular in vitro cyst-Zaprinast

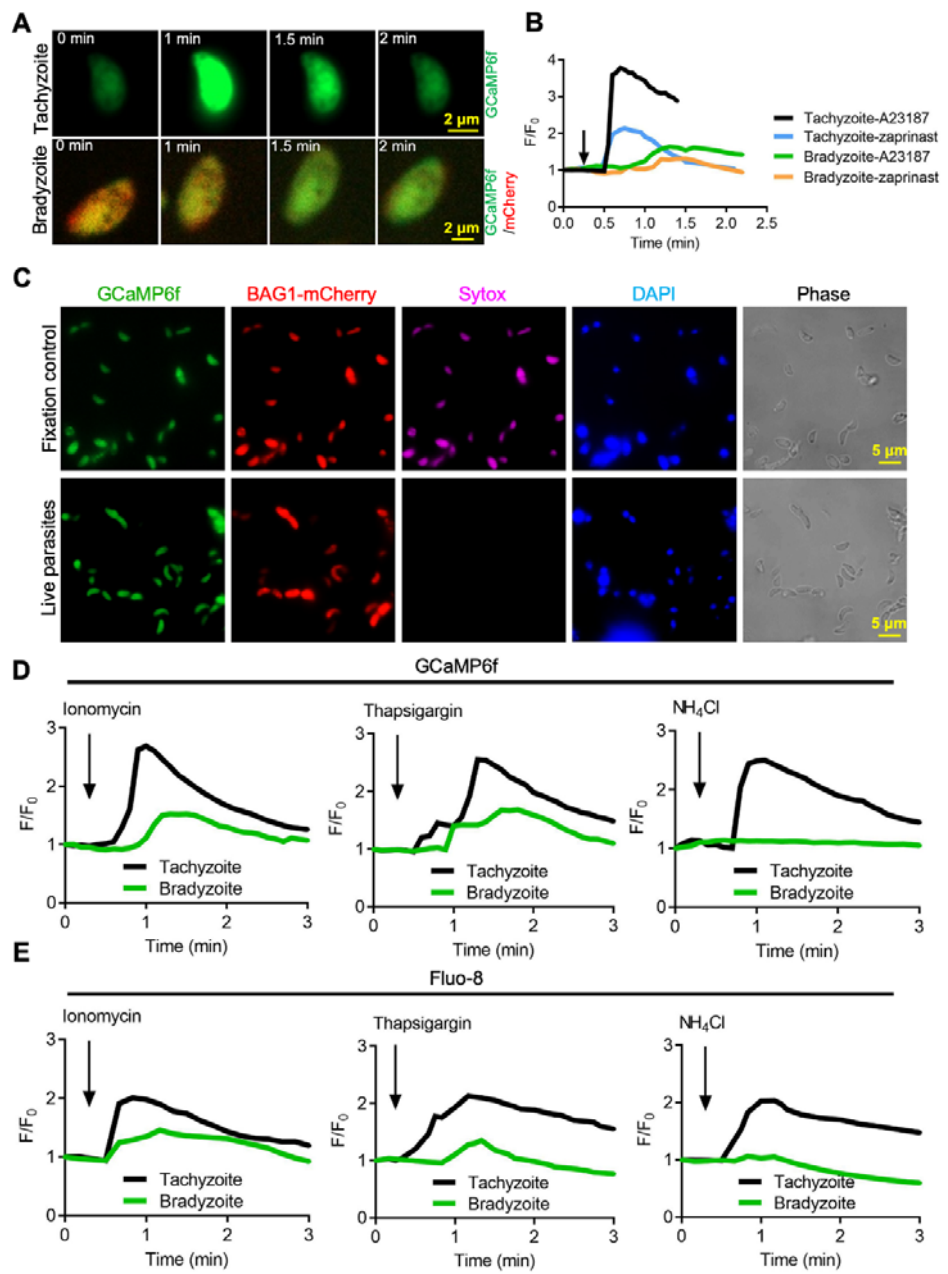


761

762 **Figure 4 figure supplement 1 Calcium responses by extracellular tachyzoites and in vitro produced**  
763 **tissue cysts**

764 (A) Fluorescence recording of ME49 strain parasites expressing GCaMP6f in response to A23187 (2  $\mu$ M) or  
765 zaprinast (500  $\mu$ M). Freshly harvested extracellular tachyzoites were compared to cysts induced in vitro in pH  
766 8.2 RPMI 1640 medium for 7 days. Arrow indicates time of addition of calcium agonists. Each kinetic curve  
767 represented the mean of 3 independent samples.

768



769

770 **Figure 5. Bradyzoites have lower  $\text{Ca}^{2+}$  stores and reduced responses to agonists compared to tachyzoites.**

771 (A) Live imaging of extracellular BAG1-mCherry GCaMP6f dual fluorescent reporter tachyzoites and

772 bradyzoites induced for 7 days at pH 8.2 in response to A23187 (2  $\mu\text{M}$ ) in EC buffer with  $\text{Ca}^{2+}$ . Bar= 2  $\mu\text{m}$ . (B)

773 Fluorescence recording of increased GCaMP6f fluorescence with  $\text{Ca}^{2+}$  increase in response to A23187 (2  $\mu\text{M}$ )

774 or zaprinast (500  $\mu\text{M}$ ) in EC buffer with  $\text{Ca}^{2+}$  for extracellular tachyzoites and bradyzoites. Arrow indicates

775 the addition of calcium agonists. Each curve is the mean of three individual parasites. (C) BAG1-mCherry

776 GCaMP6f reporter live bradyzoites were stained by SYTOX™ far red to detect dead cells and DAPI 30 min

777 after liberation from cysts. Formaldehyde-fixed bradyzoites serve as positive control. Bar= 5  $\mu\text{m}$ . (D)

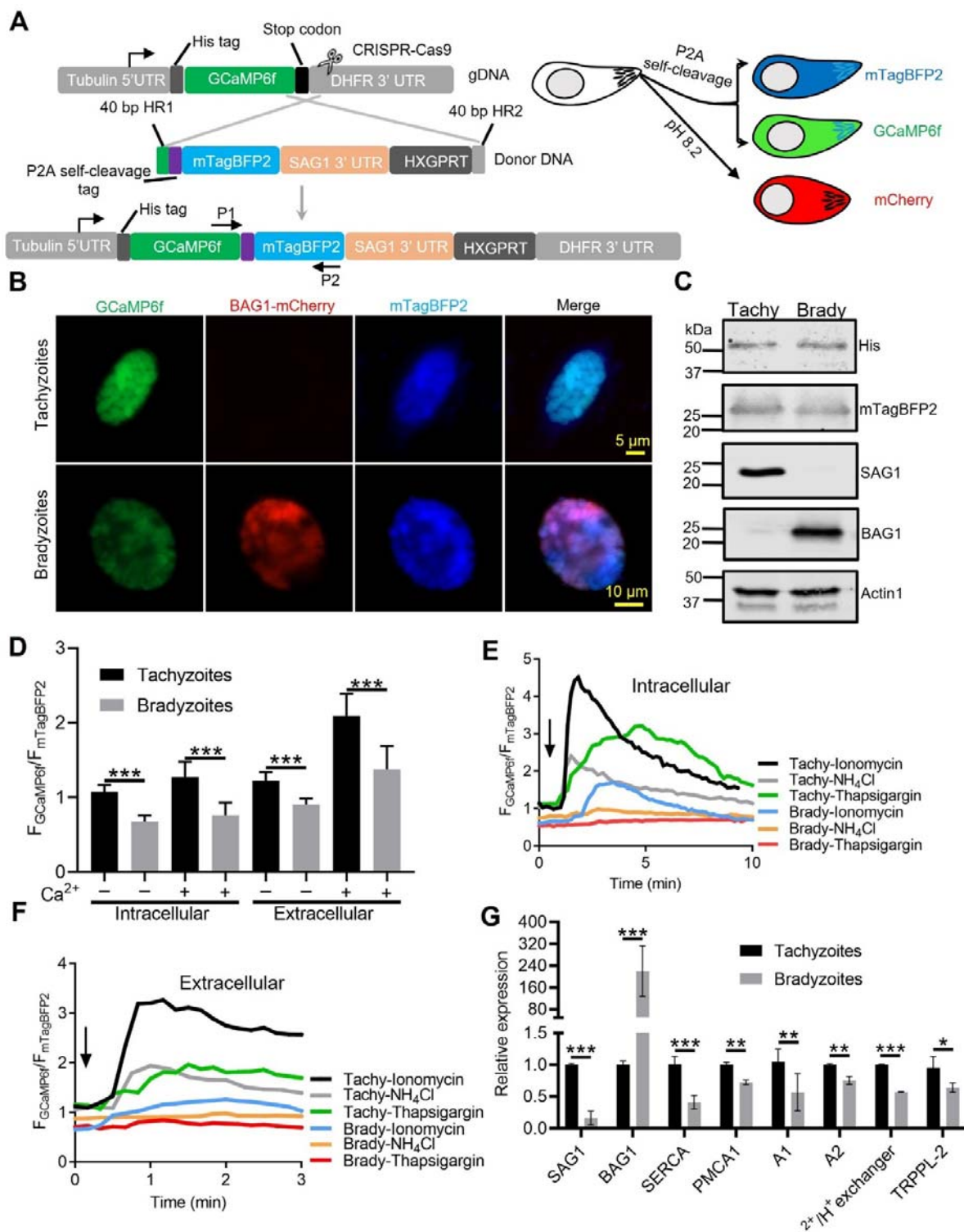
778 GCaMP6f fluorescence intensity vs. time for extracellular BAG1-mCherry GCaMP6f dual reporter parasites

779 in response to 1  $\mu\text{M}$  ionomycin, 1  $\mu\text{M}$  thapsigargin, or 10 mM  $\text{NH}_4\text{Cl}$  in EC buffer without  $\text{Ca}^{2+}$ . Arrow

780 indicates the addition of agonist. Each curve is the mean of three individual parasites. (E) Fluorescence

781 intensities change fold vs. time of extracellular BAG1-mCherry expressing bradyzoites loaded with 500 nM  
782 Fluo-8 AM after addition of 1  $\mu$ M ionomycin, 1  $\mu$ M thapsigargin or 10 mM NH<sub>4</sub>Cl in EC buffer without Ca<sup>2+</sup>.  
783 Arrow indicates the addition of agonist. Each curve is the mean of three individual parasites.

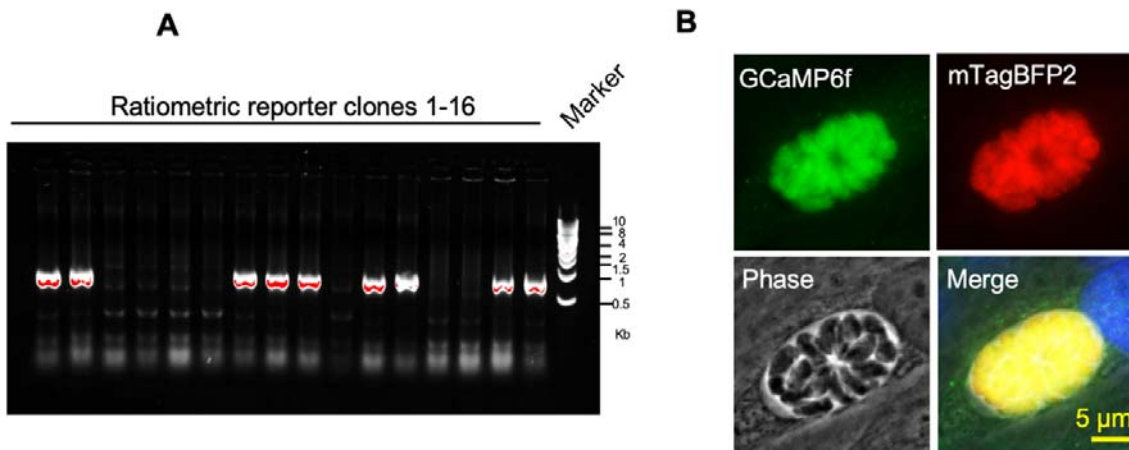
784



785 **Figure 6. Ratiometric  $\text{Ca}^{2+}$  imaging of bradyzoites reveals lower levels of resting  $\text{Ca}^{2+}$  and reduced**  
786 **response to  $\text{Ca}^{2+}$  ionophores compared to tachyzoites.** (A) Schematic diagram of generation of a  
787 ratiometric calcium reporter containing GCaMP6f fused with by a peptide P2A and blue fluorescence  
788 indicator mTagBFP2 in the background of BAG1-mCherry reporter strain. (B) Fluorescence microscopy  
789 imaging of intracellular ratiometric indicator expressed by tachyzoites cultured for 24 hr vs. bradyzoites  
790 induced for 7 days at pH 8.2 culture in EC buffer without  $\text{Ca}^{2+}$ . Bar= 10  $\mu\text{m}$ . (C) Western blots showing  
791

792 GCaMP6f and mTagBFP2 produced from the ratiometric reporter expressed by tachyzoites and bradyzoite.  
793  $\alpha$ His and  $\alpha$ tRFP antibodies were used to probe the expression of GCaMP6f and mTagBFP2, respectively.  
794 SAG1 and BAG1 serve as the stage-specific marker of tachyzoites and bradyzoites, respectively. Actin  
795 functions as loading control. (D) Quantification of basal calcium levels normalized by comparison of  
796 GCaMP6f to mTagBFP2 fluorescence intensity ratios of intracellular and extracellular tachyzoites or  
797 bradyzoites that were induced by culture for 7 days at pH 8.2. For extracellular parasites, tachyzoites were  
798 liberated mechanically and bradyzoites were liberated by trypsin treatment. Parasites within intact cells, or  
799 extracellular parasites were incubated in EC buffer with or without  $\text{Ca}^{2+}$  for 10 min before imaging. Data  
800 represent mean values from two independent experiments with 10 total vacuoles or cysts for each treatment.  
801 Two-tailed unpaired Student's t test, \*\*\*,  $P < 0.001$ . (E) Monitoring of GCaMP6f/ mTagBFP2 fluorescence  
802 intensity ratio vs. time for intracellular tachyzoites and in vitro induced bradyzoites that were induced by  
803 culture for 7 days at pH 8.2. (F) For extracellular parasites, tachyzoites were liberated mechanically and  
804 bradyzoites were liberated by trypsin treatment. Parasites were incubated in EC buffer without  $\text{Ca}^{2+}$  for 10  
805 min and responses were measured to ionomycin (1  $\mu\text{M}$ ), thapsigargin (1  $\mu\text{M}$ ) or 10 mM  $\text{NH}_4\text{Cl}$ . Arrow  
806 indicates time of addition of agonists. Each kinetic curve represents mean data of 3 independent samples  
807 (individual vacuoles or cysts for intracellular and single parasites for extracellular). (G) Gene expression  
808 levels in tachyzoites and bradyzoites induced for 7 days at pH 8.2. mRNA levels were measured using  
809 RT-PCR and expressed relative to the housekeeping transcript for actin. SAG1 and BAG1 were used to  
810 monitor tachyzoites and bradyzoites, respectively. Data represent the mean  $\pm$  SD of two independent assays  
811 containing triplicate samples each. Multiple Student's t tests, \*\*,  $P < 0.01$ , \*\*\*,  $P < 0.001$ .

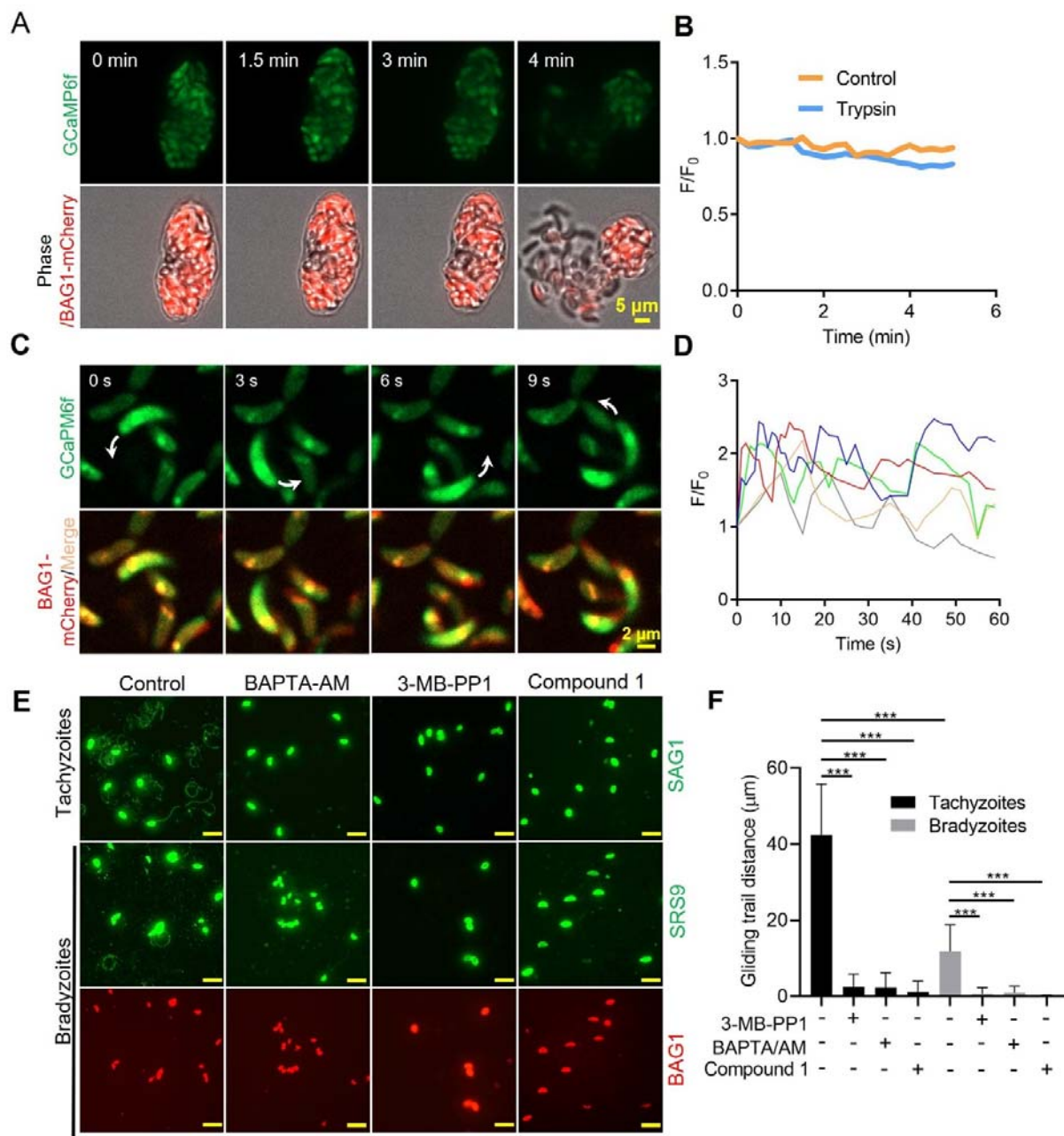
812



813  
814 **Figure 6 figure supplement 1 Identification of ME49 GCaMP6f-P2A-mTagBFP2 BAG1-mCherry**  
815 **ratiometric reporter by PCR and IFA**

816 (A) Transgenic screening of clones of ME49 GCaMP6f BAG1-mCherry parasites expressing P2A-mTagBFP2  
817 at the C-terminal of GCaMP6f using PCR amplification with primer set P1-P2 shown in diagram in **Figure**  
818 **6A.** (B) IFA analysis showing co-localization of GCaMP6f and mTagBFP2 in tachyzoites of the dual reporter  
819 strain grown in HFF cells for 24 hr. Monoclonal anti-His antibody was used to stain GCaMP6f while rabbit  
820 anti-tRFP antibody was used to stain mTagBFP2 followed by goat anti-mouse IgG conjugated to Alexa  
821 Fluor-488 and goat anti-rabbit IgG conjugated to Alexa Fluor-568 secondary antibodies. Scale bar = 5  $\mu$ m.

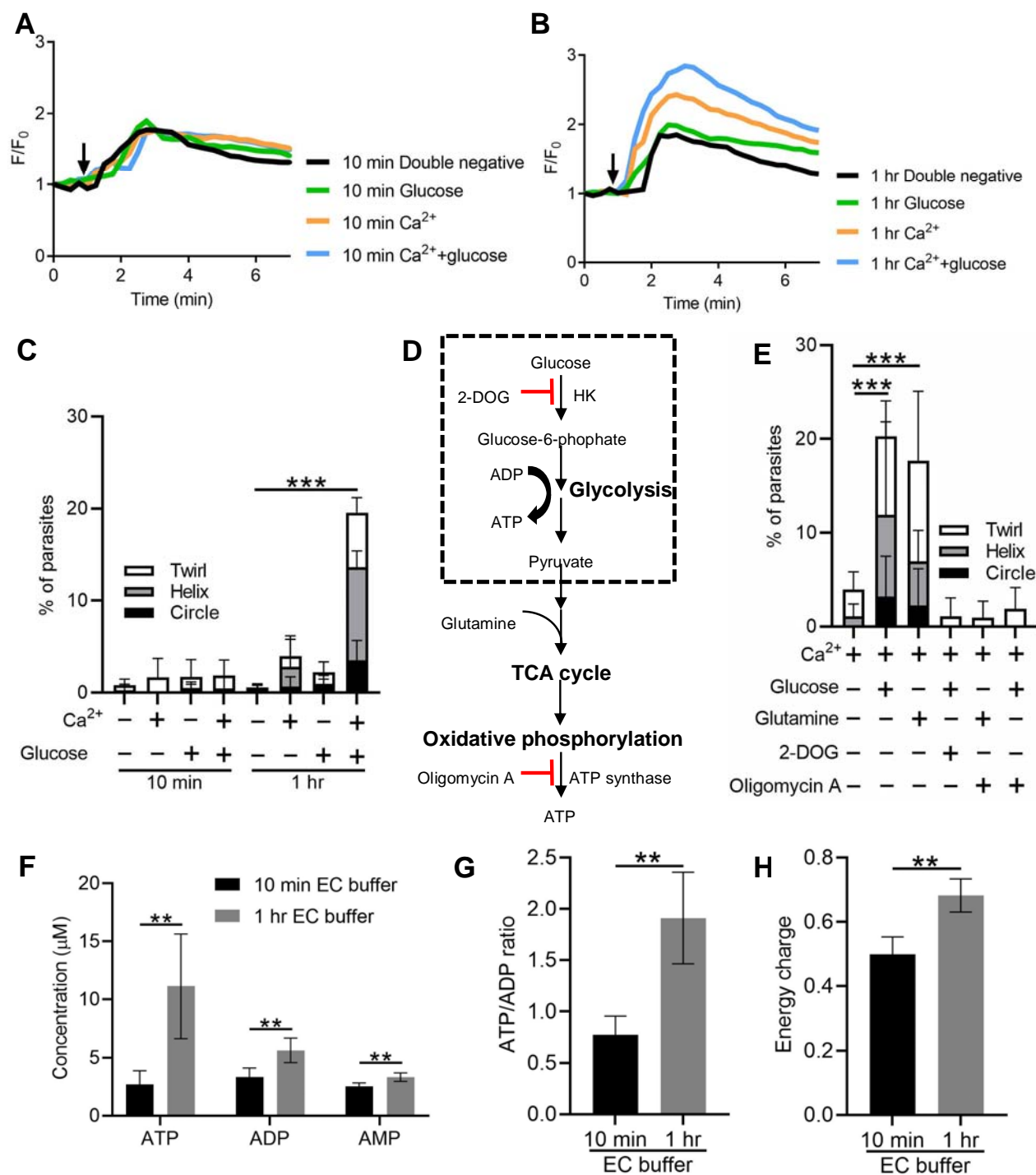
822



824 **Figure 7.  $\text{Ca}^{2+}$  signaling governs gliding motility of bradyzoites.** (A) Time-lapse microscopy recording  
825 GCaMP6f BAG1-mCherry bradyzoites induced for 7 days at pH 8.2. Cells were imaged during the digestion  
826 by 0.25 mg/ml Trypsin for 5 min in EC buffer with 1.8 mM  $\text{Ca}^{2+}$ . Bar = 5  $\mu$ m. (B) GCaMP6f fluorescence  
827 change ratio vs. time of BAG1-mCherry GCaMP6f bradyzoites induced for 7 days at pH 8.2 treated with or  
828 without trypsin. Curves represent mean data from 3 independent cysts. (C) Spinning disc confocal microscopy  
829 monitoring circular gliding motility of bradyzoites liberated by 0.25 mg/ml trypsin for 10 min from cysts  
830 induced for 7 days at pH 8.2. Arrow shows the direction of gliding motility by one bradyzoite. Bar = 5  $\mu$ m. (D)  
831  $\text{Ca}^{2+}$  kinetics of bradyzoites undergoing gliding motility after liberation from cysts induced for 7 days at pH  
832 8.2. The graph shows fluctuated  $\text{Ca}^{2+}$  kinetics of 5 independent single bradyzoites. (E) Indirect  
833 immunofluorescence microscopy showing the trails of parasites during gliding motility. Parasites were treated  
834 with DMSO (control), 5  $\mu$ M 3-MB-PP1, 25  $\mu$ M BAPTA-AM and 4  $\mu$ M Compound 1. Anti-SAG1 mAb DG52

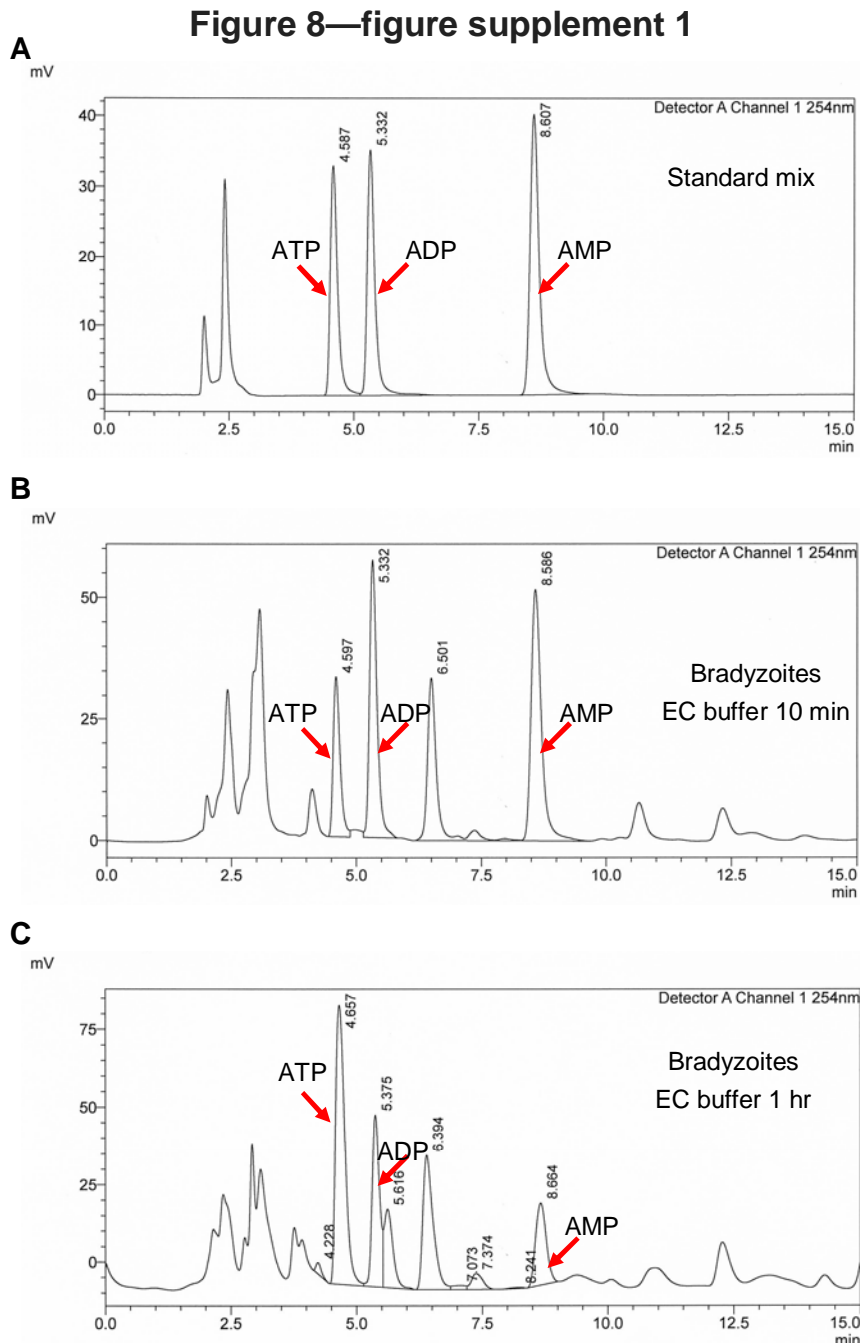
835 and rabbit polyclonal anti-SRS9 antibodies followed by secondary antibodies conjugated to goat anti-mouse  
836 IgG Alexa 488 were used to stain the gliding trails of tachyzoites and bradyzoites, respectively. Anti-BAG1  
837 followed by goat anti-rabbit IgG conjugated of Alexa 568 served as marker of bradyzoites. Bar=10  $\mu$ m. (F)  
838 Quantification of trails from gliding motility of tachyzoites and bradyzoites treated with DMSO (control), 5  
839  $\mu$ M 3-MB-PP1, 25  $\mu$ M BAPTA-AM and 4  $\mu$ M compound 1. Data represented as means  $\pm$  SEM ((n = 20  
840 replicates combined from n = 3 independent experiments). Kruskal-Wallis test with Dun's multiple  
841 comparison correction \*\*\*,  $P < 0.001$ .

842



843 **Figure 8. Exogenous  $\text{Ca}^{2+}$  and glucose collectively contributes to bradyzoites gliding motility via**  
844 **refilling calcium pools and increasing ATP production.** (A-B) Monitoring the relative intensity of  
845 GCaMP6f fluorescence fold change ( $F/F_0$ ) vs. time from extracellular bradyzoites treated with  $1 \mu\text{M}$   
846 ionomycin. Bradyzoites induced for 7 days at pH 8.2 were released from in vitro cysts by  $0.25 \text{ mg/ml}$  trypsin  
847 and pre-incubated in EC buffer  $\pm 1.8 \text{ mM } \text{Ca}^{2+}$  and /or  $\pm 5.6 \text{ mM}$  glucose for 10 min (A) or 1 hr (B) before  
848 measurements. Each kinetic curve represents mean data of 3 extracellular parasites. Arrow indicates the  
849 addition of  $1 \mu\text{M}$  ionomycin. Double negative refers to the absence of  $\text{Ca}^{2+}$  and glucose. (C) Percentage of

850 extracellular parasites undergoing different forms of gliding motility as determined from time-lapse video  
851 microscopy. Bradyzoites induced for 7 days at pH 8.2 were treated in EC buffer  $\pm$  1.8 mM Ca<sup>2+</sup> and/or  $\pm$  5.6  
852 mM glucose for 10 min or 1 hr before measurements. Means  $\pm$  SD of two independent experiments with 6  
853 replicates each. Kruskal-Wallis test with Dunn's multiple comparison correction test \*\*\*,  $P < 0.001$  for  
854 comparison between – calcium / - glucose and + calcium / + glucose. All other groups were not significantly  
855 different from the negative control. (D) Schematic illustration of mechanism of 2-deoxyglucose (2-DOG) and  
856 oligomycin A in inhibiting ATP production. (E) Percentage of bradyzoites with different forms of gliding  
857 motility determined by time-lapse video microscopy. Bradyzoites induced for 7 days at pH 8.2 were treated in  
858 EC buffer (1.8 mM Ca<sup>2+</sup>)  $\pm$  5.6 mM glucose, 5.6 mM glutamine, 50 mM 2-DOG, or 20  $\mu$ M oligomycin A for  
859 1 hr before measurements. Means  $\pm$  SD of two independent experiments with 6 replicates each.  
860 Kruskal-Wallis test with Dunn's multiple comparison correction test \*\*\*,  $P < 0.001$ . (F-H) High-performance  
861 liquid chromatography UV (HPLC-UV) analysis of ATP, ADP and AMP levels in extracellular bradyzoites  
862 incubated with EC buffer containing 1.8 mM Ca<sup>2+</sup> and 5.6 mM glucose for 10 min or 1 hr. Bradyzoites induced  
863 for 7 days at pH 8.2 were purified by magnetic beads and released from in vitro cysts by 0.25 mg/ml trypsin.  
864 Data from two independent experiments with 6 technical replicates. (F) Concentrations of ATP, ADP, and AMP  
865 in extracellular bradyzoites represented as mean  $\pm$  SD. Multiple Student's t tests, \*\*,  $P < 0.01$ . (G) ATP/ADP  
866 ratios in extracellular bradyzoites represented as mean  $\pm$  SD. Two-tailed Mann-Whitney test, \*\*,  $P < 0.01$ . (H)  
867 Energy charge of extracellular bradyzoites calculated as [ATP]+0.5x[ADP]/[ATP]+[ADP]+[AMP] represented  
868 as mean  $\pm$  SD Two-tailed Mann-Whitney test, \*\*.  $P \leq 0.01$ .



869 **Figure 8 figure supplement 1** Establishment of HPLC-UV analysis of ATP, ADP and AMP levels in  
870 parasites

871 (A) HPLC-UV chromatograms of standard mix containing 12.5  $\mu$ M ATP, 12.5  $\mu$ M ADP and 12.5  $\mu$ M AMP.  
872 Arrows indicate the peaks of ATP, ADP and AMP. (B) HPLC-UV chromatograms of ATP, ADP and AMP  
873 extracts from bradyzoites ( $2 \times 10^7$ ) incubated with EC buffer containing 1.8 mM  $\text{Ca}^{2+}$  and 5.6 mM glucose for  
874 10 min. Arrows indicate the peaks of ATP, ADP and AMP. (C) HPLC-UV chromatograms of ATP, ADP and  
875 AMP extracts from bradyzoites ( $1.2 \times 10^7$ ) incubated with EC buffer containing 1.8 mM  $\text{Ca}^{2+}$  and 5.6 mM  
876 glucose for 1 hr. Arrows indicate the peaks of ATP, ADP and AMP.

877

878 **Rich Media Files**

879 **Figure 1-video 1 Egress by ME49 BAG1-mCherry tachyzoites in response to A23187.**

880 Time-lapse video microscopy showing A23187 (2  $\mu$ M) induced egress of ME49 BAG1-mCherry strain  
881 tachyzoites grown in vitro in HFF cells for 24 hr. Videos for intracellular tachyzoites in EC buffer were  
882 recorded for 10 min and A23187 (2  $\mu$ M) was added 30 s after the recording initiated. Display frame rate is 8  
883 frames per second while the acquisition frame rate is 3 frames per second. Bar = 10  $\mu$ m.

884 **Figure 1-video 2 Egress by ME49 BAG1-mCherry bradyzoites in response to A23187.**

885 Time-lapse video microscopy showing A23187 (2  $\mu$ M) induced egress of ME49 BAG1-mCherry strain  
886 bradyzoites induced by in vitro culture on HFF cells for 7 days at pH 8.2. Videos for intracellular bradyzoites  
887 in EC buffer were recorded for 10 min and A23187 (2  $\mu$ M) was added 30 s after the recording initiated.  
888 Display frame rate is 4 frames per second while the acquisition frame rate is 10 frames per second. Bar = 10  
889  $\mu$ m.

890 **Figure 2-video 1 A23187 - induced permeabilization of the parasitophorous vacuole membrane (PVM)  
891 detected by vacuolar leakage of FNR-mCherry secreted by tachyzoites.**

892 Time-lapse video microscopy showing A23187 (2  $\mu$ M)-induced FNR-mCherry leakage from the PV  
893 surrounding FNR-mCherry BAG1-EGFP expressing tachyzoites. FNR-mCherry BAG1-EGFP tachyzoites  
894 cultured under normal condition in HFF cells for 24 hr were treated with A23187 (2  $\mu$ M) in EC buffer for 10  
895 min at 37°C. Videos were recorded for 10 min and A23187 (2  $\mu$ M) was added 30 s after the recording initiated.  
896 Display frame rate is 6 frames per second while the acquisition frame rate is 5 frames per second. Bar = 5  $\mu$ m.

897 **Figure 2-video 2 Trypsin - induced disruption of in vitro differentiated tissue cysts expressing ME49  
898 FNR-mCherry BAG1-EGFP.**

899 Time-lapse video microscopy showing A23187-induced FNR-mCherry leakage in vitro differentiated tissue  
900 cysts of FNR-mCherry BAG1-EGFP bradyzoites. FNR-mCherry BAG1-EGFP bradyzoites induced by  
901 cultivation in HFF cells in vitro for 7 days at pH 8.2 were treated with 0.25 mg/ml Trypsin in EC buffer for 6  
902 min at 37°C. Videos were recorded for 6 min and 0.25 mg/ml Trypsin was added 30 s after the recording  
903 initiated. Display frame rate is 3 frames per second while the acquisition frame rate is 15 frames per second.  
904 Bar = 5  $\mu$ m.

905 **Figure 2-video 3 A23187 -induced permeabilization of in vitro differentiated tissue cysts detected by  
906 vacuolar FNR-mCherry leakage from ME49 FNR-mCherry BAG1-EGFP bradyzoites.**

907 Time-lapse video microscopy showing A23187 (2  $\mu$ M)-induced FNR-mCherry leakage from in vitro  
908 differentiated cysts of FNR-mCherry BAG1-EGFP. FNR-mCherry BAG1-EGFP bradyzoites induced by  
909 cultivation in HFF cells in vitro for 7 days at pH 8.2 were treated with A23187 (2  $\mu$ M) in EC buffer for 10 min  
910 at 37°C. Videos were recorded for 10 min and A23187 (2  $\mu$ M) was added 30 s after the recording initiated.  
911 Display frame rate is 3 frames per second while the acquisition frame rate is 15 frames per second. Bar = 5  
912  $\mu$ m.

913 **Figure 3-video 1 Calcium response of ME49 BAG1-Cherry GCaMP6f expressing tachyzoites stimulated  
914 by A23187.**

915 Time-lapse video microscopy showing GCaMP6f fluorescence changes of intracellular ME49 BAG1-mCherry  
916 GCaMP6f tachyzoites grown in HFF cells in vitro for 24 hr in response to A23187 (2  $\mu$ M) in EC buffer.  
917 Videos were recorded for 10 min and A23187 (2  $\mu$ M) was added 30 s after the recording initiated. Display  
918 frame rate is 10 frames per second while the acquisition frame rate is 3 frames per second. Bar = 10  $\mu$ m.

919 **Figure 3-video 2 Calcium response of ME49 BAG1-Cherry GCaMP6f expressing bradyzoites  
920 stimulated by A23187.**

921 Time-lapse video microscopy showing GCaMP6f fluorescence changes of intracellular ME49 BAG1-mCherry  
922 GCaMP6f bradyzoites induced by cultivation in HFF cells in vitro for 7 days at pH 8.2 in response to A23187  
923 (2  $\mu$ M) in EC buffer. Videos were recorded for 14 min and A23187 (2  $\mu$ M) was added 30 s after the recording  
924 initiated. Display frame rate is 6 frames per second while the acquisition frame rate is 10 frames per second.  
925 Bar = 10  $\mu$ m.

926 **Figure 4-video 1 Calcium response of ME49 BAG1-mCherry GCaMP6f cysts isolated from chronically  
927 infected mouse brains and treated in vitro with DMSO.**

928 Time-lapse video microscopy showing GCaMP6f fluorescence changes of ME49 BAG1-mCherry GCaMP6f  
929 cysts isolated 30 days post-infection from the brains of chronically infected mice in response to DMSO (0.1%)  
930 in EC buffer. Videos were recorded for 5 min and DMSO (0.1%) was added 15 s after the recording initiated.  
931 Display frame rate is 6 frames per second while the acquisition frame rate is 3 frames per second. Bar = 2  $\mu$ m.

932 **Figure 4-video 2 Calcium response of ME49 BAG1-mCherry GCaMP6f cysts isolated from chronically  
933 infected mouse brains and treated in vitro with A23187.**

934 Time-lapse video microscopy showing GCaMP6f fluorescence changes of ME49 BAG1-mCherry GCaMP6f  
935 cysts isolated 30 days post-infection from chronically infected mice in response to A23187 (2  $\mu$ M) in EC  
936 buffer. Videos were recorded for 5 min and A23187 (2  $\mu$ M) was added 15 s after the recording initiated.  
937 Display frame rate is 6 frames per second while the acquisition frame rate is 5 frames per second. Bar = 2  $\mu$ m.

938 **Figure 5-video 1 Calcium response of extracellular ME49 BAG1-mCherry GCaMP6f tachyzoite in**  
939 **response to A23187.**

940 Time-lapse video microscopy showing GCaMP6f fluorescence changes of extracellular ME49  
941 BAG1-mCherry GCaMP6f tachyzoite in response to A23187 (2  $\mu$ M) in EC buffer. Videos were recorded for 3  
942 min and A23187 (2  $\mu$ M) was added 15 s after the recording initiated. Display frame rate is 4 frames per  
943 second while the acquisition frame rate is 3 frames per second. Bar = 2  $\mu$ m.

944 **Figure 5-video 2 Calcium response of extracellular ME49 BAG1-mCherry GCaMP6f bradyzoite in**  
945 **response to A23187.**

946 Time-lapse video microscopy showing GCaMP6f fluorescence changes of extracellular ME49  
947 BAG1-mCherry GCaMP6f bradyzoite in response to A23187 (2  $\mu$ M) in EC buffer. Bradyzoites were liberated  
948 by 0.25 mg/ml trypsin for 5 min from in vitro cysts induced for cultivation in HFF cells for 7 days at pH 8.2.  
949 Videos were recorded for 3 min and A23187 (2  $\mu$ M) was added 15 s after the recording initiated. Display  
950 frame rate is 2 frames per second while the acquisition frame rate is 5 frames per second. Bar = 2  $\mu$ m.

951 **Figure 7-video 1 Trypsin induced liberation of ME49 BAG1-mCherry GCaMP6f bradyzoites from in**  
952 **vitro cultured cysts.**

953 Time-lapse video microscopy recording GCaMP6f fluorescence changes from BAG1-mCherry GCaMP6f  
954 bradyzoites induced by cultivation in HFF cells for 7 days at pH 8.2 during digestion by 0.25 mg/ml Trypsin  
955 in EC buffer. Videos were recorded for 6 min and 0.25 mg/ml trypsin was added 30 s after the recording  
956 initiated. Display frame rate is 16 frames per second while the acquisition frame rate is 5 frames per second.  
957 Bar = 5  $\mu$ m.

958 **Figure 7-video 2 Gliding motility of ME49 BAG1-mCherry GCaMP6f bradyzoites released from in**  
959 **vitro cysts.**

960 Time-lapse video microscopy of gliding motility of bradyzoites liberated by 0.25 mg/ml trypsin for 5 min  
961 from in vitro cyst induced by cultivation in HFF cells for 7 days at pH 8.2. Images were collected using  
962 spinning disc confocal microscopy. The arrow shows the gliding motility of bradyzoite in EC buffer. Videos  
963 were recorded for 2 min. Display frame rate is 6 frames per second while the acquisition frame rate is 1 frame  
964 per second. Bar = 2  $\mu$ m.

965

966 **Supplementary Files**

967 Supplementary Table 1: Primers used in this study

968 Supplementary Table S2 Plasmids used in this study

969 Supplementary Table S3 Parasite lines used in this study

970

971 **References**

972

- 973 1. Dubey JP (2010) *Toxoplasmosis of animals and humans*. Boca Raton: CRC Press. 313 p.
- 974 2. Jones JL, Dubey JP (2012) *Foodborne Toxoplasmosis*. Clin Infect Dis 55: 864-851.
- 975 3. Jones JL, Dubey JP (2010) Waterborne toxoplasmosis--recent developments. Exp Parasitol 124: 10-25.
- 976 4. Drewry LL, Sibley LD (2019) The hitchhiker's guide to parasite dissemination. Cell Microbiol: e13070.
- 977 5. Watts E, Zhao Y, Dhara A, Eller B, Patwardhan A, et al. (2015) Novel Approaches Reveal that *Toxoplasma gondii*  
978 Bradyzoites within Tissue Cysts Are Dynamic and Replicating Entities In Vivo. MBio 6: e01155-01115.
- 979 6. Jeffers V, Tampaki Z, Kim K, Sullivan WJ, Jr. (2018) A latent ability to persist: differentiation in *Toxoplasma gondii*. Cell  
980 Mol Life Sci 75: 2355-2373.
- 981 7. Mayoral J, Di Cristina M, Carruthers VB, Weiss LM (2020) *Toxoplasma gondii*: Bradyzoite Differentiation In Vitro and In  
982 Vivo. Methods Mol Biol 2071: 269-282.
- 983 8. Lourido S, Moreno SN (2015) The calcium signaling toolkit of the Apicomplexan parasites *Toxoplasma gondii* and  
984 *Plasmodium* spp. Cell Calcium 57: 186-193.
- 985 9. Carruthers VB, Sibley LD (1999) Mobilization of intracellular calcium stimulates microneme discharge in *Toxoplasma*  
986 *gondii*. Mol Microbiol 31: 421-428.
- 987 10. Carruthers VB, Moreno SNJ, Sibley LD (1999) Ethanol and acetaldehyde elevate intracellular  $[Ca^{2+}]$  calcium and  
988 stimulate microneme discharge in *Toxoplasma gondii*. Biochem J 342: 379-386.
- 989 11. Wetzel DM, Chen LA, Ruiz FA, Moreno SNJ, Sibley LD (2004) Calcium-mediated protein secretion potentiates motility  
990 by *Toxoplasma gondii*. J Cell Sci 117: 5739-5748.
- 991 12. Lovett JL, Marchesini N, Moreno SN, Sibley LD (2002) *Toxoplasma gondii* microneme secretion involves intracellular  
992  $Ca^{2+}$  release from  $IP_3$  / ryanodine sensitive stores. J Biol Chem 277: 25870-25876.
- 993 13. Vieira MCF, Moreno SNJ (2000) Mobilization of intracellular calcium upon attachment of *Toxoplasma gondii*  
994 tachyzoites to human fibroblasts is required for invasion. Molec Biochem Parasit 106: 157-162.
- 995 14. Pace DA, McKnight CA, Liu J, Jimenez V, Moreno SN (2014) Calcium entry in *Toxoplasma gondii* and its enhancing  
996 effect of invasion-linked traits. J Biol Chem.
- 997 15. Kafsack BF, Pena JD, Coppens I, Ravindran S, Boothroyd JC, et al. (2009) Rapid membrane disruption by a  
998 perforin-like protein facilitates parasite exit from host cells. Science 323: 530-533.
- 999 16. Brown KM, Sibley LD (2018) Essential cGMP Signaling in *Toxoplasma* Is Initiated by a Hybrid P-Type  
1000 ATPase-Guanylate Cyclase. Cell Host Microbe 24: 804-816 e806.
- 1001 17. Bisio H, Lunghi M, Brochet M, Soldati-Favre D (2019) Phosphatidic acid governs natural egress in *Toxoplasma gondii*  
1002 via a guanylate cyclase receptor platform. Nat Microbiol 4: 420-428.
- 1003 18. Yang L, Ubaldi AD, Seizova S, Wilde ML, Coffey MJ, et al. (2019) An apically located hybrid guanylate cyclase-ATPase  
1004 is critical for the initiation of  $Ca(2+)$  signaling and motility in *Toxoplasma gondii*. J Biol Chem 294: 8959-8972.
- 1005 19. Brown KM, Long S, Sibley LD (2017) Plasma membrane association by N-acylation governs PKG function in  
1006 *Toxoplasma gondii*. mBio 8(3): e00375-00317.
- 1007 20. Fang J, Marchesini N, Moreno SNJ (2006) A *Toxoplasma gondii* phosphoinositide phospholipase C (TgPI-PLC) with  
1008 high affinity for phosphatidylinositol. Biochem J 394: 417-425.
- 1009 21. Bullen HE, Jia Y, Yamaryo-Botte Y, Bisio H, Zhang O, et al. (2016) Phosphatidic Acid-Mediated Signaling Regulates  
1010 Microneme Secretion in *Toxoplasma*. Cell Host Microbe 19: 349-360.
- 1011 22. Balestra AC, Koussis K, Klages N, Howell SA, Flynn HR, et al. (2021)  $Ca(2+)$  signals critical for egress and  
1012 gametogenesis in malaria parasites depend on a multipass membrane protein that interacts with PKG. Sci Adv  
1013 7.
- 1014 23. Lourido S, Tang K, Sibley LD (2012) Distinct signalling pathways control *Toxoplasma* egress and host-cell invasion.  
1015 EMBO J 31: 4524-4534.

1016 24. McCoy JM, Whitehead L, van Dooren GG, Tonkin CJ (2012) TgCDPK3 regulates calcium-dependent egress of  
1017 *Toxoplasma gondii* from host cells. PLoS Pathog 8: e1003066.

1018 25. Tagoe DNA, Drozda AA, Falco JA, Bechtel TJ, Weerapana E, et al. (2021) Ferlins and TgDOC2 in Toxoplasma  
1019 Microneme, Rhopty and Dense Granule Secretion. Life (Basel) 11.

1020 26. Long S, Brown KM, Drewry LL, Anthony B, Phan I, et al. (2017) Calmodulin-like proteins localized to the conoid  
1021 regulate motility and cell invasion by *Toxoplasma gondii*. PloS Pathogens 13: e1006379.

1022 27. Jia Y, Marq JB, Bisio H, Jacot D, Mueller C, et al. (2017) Crosstalk between PKA and PKG controls pH-dependent host  
1023 cell egress of *Toxoplasma gondii*. EMBO J 36: 3250-3267.

1024 28. Uboldi AD, Wilde ML, McRae EA, Stewart RJ, Dagley LF, et al. (2018) Protein kinase A negatively regulates Ca<sup>2+</sup>  
1025 signalling in *Toxoplasma gondii*. PLoS Biol 16: e2005642.

1026 29. Brown KM, Tonkin CJ, Billker O, Sibley LD (2019) Calcium and cyclic nucleotide signaling networks in *Toxoplasma*  
1027 *gondii*. In: Weiss LM, Kim K, editors. *Toxoplasma gondii: The Model Apicomplexan: Perspectives and Methods*.  
1028 3rd ed: Academic Press. pp. in press.

1029 30. Hortua Triana MA, Marquez-Nogueras KM, Vella SA, Moreno SNJ (2018) Calcium signaling and the lytic cycle of the  
1030 Apicomplexan parasite *Toxoplasma gondii*. Biochim Biophys Acta Mol Cell Res 1865: 1846-1856.

1031 31. Nagamune K, Sibley LD (2006) Comparative genomic and phylogenetic analyses of calcium ATPases and  
1032 calcium-regulated proteins in the Apicomplexa. Molec Biol Evol 23: 1613-1627.

1033 32. Prole DL, Taylor CW (2011) Identification of intracellular and plasma membrane calcium channel homologues in  
1034 pathogenic parasites. PLoS One 6: e26218.

1035 33. Thastrup O, Cullen PJ, Drobak BK, Hanley MR, Dawson AP (1990) Thapsigargin, a tumor promotor, discharges  
1036 intracellular Ca<sup>2+</sup> stores by specific inhibition of the endoplasmic reticulum Ca<sup>2+</sup>-ATPase. Proc Natl Acad Sci USA  
1037 87: 2766-2470.

1038 34. Nagamune K, Moreno SNJ, Sibley LD (2007) Artemisinin resistant mutants of *Toxoplasma gondii* have altered calcium  
1039 homeostasis. Anti Microb Agents Chemother 51: 3816-3823.

1040 35. Moreno SNJ, Zhong L (1996) Acidocalcisomes in *Toxoplasma gondii* tachyzoites. Biochemical Journal 313: 655-659.

1041 36. Luo S, Ruiz FA, Moreno SN (2005) The acidocalcisome Ca<sup>2+</sup> ATPase (TgA1) of *Toxoplasma gondii* is required for  
1042 polyphosphate storage, intracellular calcium homeostasis and virulence. Molec Micro 55: 1034-1045.

1043 37. Vella SA, Moore CA, Li ZH, Hortua Triana MA, Potapenko E, et al. (2021) The role of potassium and host calcium  
1044 signaling in *Toxoplasma gondii* egress. Cell Calcium 94: 102337.

1045 38. Vella SA, Calixto A, Asady B, Li ZH, Moreno SNJ (2020) Genetic Indicators for Calcium Signaling Studies in *Toxoplasma*  
1046 *gondii*. Methods Mol Biol 2071: 187-207.

1047 39. Lovett JL, Sibley LD (2003) Intracellular calcium stores in *Toxoplasma gondii* govern invasion of host cells. J Cell Sci  
1048 116: 3009-3016.

1049 40. Sidik SM, Hortua Triana MA, Paul AS, El Bakkouri M, Hackett CG, et al. (2016) Using a Genetically Encoded Sensor to  
1050 Identify Inhibitors of *Toxoplasma gondii* Ca<sup>2+</sup> Signaling. J Biol Chem 291: 9566-9580.

1051 41. Borges-Pereira L, Budu A, McKnight CA, Moore CA, Vella SA, et al. (2015) Calcium Signaling throughout the  
1052 *Toxoplasma gondii* Lytic Cycle: A STUDY USING GENETICALLY ENCODED CALCIUM INDICATORS. J Biol Chem 290:  
1053 26914-26926.

1054 42. Brown KM, Lourido S, Sibley LD (2016) Serum Albumin Stimulates Protein Kinase G-dependent Microneme Secretion  
1055 in *Toxoplasma gondii*. J Biol Chem 291: 9554-9565.

1056 43. Ferguson DJP, Hutchison WM, Pettersen E (1989) Tissue cyst rupture in mice chronically infected with *Toxoplasma*  
1057 *gondii*. Parasitol Res 75: 599-603.

1058 44. Frenkel JK, Escajadillo A (1987) Cyst rupture as a pathogenic mechanism of toxoplasmic encephalitis. American  
1059 Journal of Tropical Medicine and Hygiene 36: 517-522.

1060 45. Hofflin JM, Conley FK, Remington JS (1987) Murine model of intracerebral toxoplasmosis. Journal of Infectious  
1061 Diseases 155: 550-556.

1062 46. Soête M, Fortier B, Camus D, Dubremetz JF (1993) *Toxoplasma gondii*: kinetics of bradyzoite-tachyzoite

1063 interconversion *in vitro*. *Exp Parasitol* 76: 259-264.

1064 47. Swierzy IJ, Luder CG (2015) Withdrawal of skeletal muscle cells from cell cycle progression triggers differentiation of  
1065 Toxoplasma gondii towards the bradyzoite stage. *Cell Microbiol* 17: 2-17.

1066 48. Halonen SK, Lyman WD, Chiu FC (1996) Growth and development of *Toxoplasma gondii* in human neurons and  
1067 astrocytes. *J Neuropathology and Exp Neurology* 55: 1150-1156.

1068 49. White MW, Radke JR, Radke JB (2014) Toxoplasma development - turn the switch on or off? *Cell Microbiol* 16:  
1069 466-472.

1070 50. Beeler TJ, Jona I, Martonosi A (1979) The effect of ionomycin on calcium fluxes in sarcoplasmic reticulum vesicles  
1071 and liposomes. *J Biol Chem* 254: 6229-6231.

1072 51. Lourido S, Shuman J, Zhang C, Shokat KM, Hui R, et al. (2010) Calcium-dependent protein kinase 1 is an essential  
1073 regulator of exocytosis in Toxoplasma. *Nature* 465: 359-362.

1074 52. Cranfill PJ, Sell BR, Baird MA, Allen JR, Lavagnino Z, et al. (2016) Quantitative assessment of fluorescent proteins. *Nat  
1075 Methods* 13: 557-562.

1076 53. Marquez-Nogueras KM, Hortua Triana MA, Chasen NM, Kuo IY, Moreno SN (2021) Calcium signaling through a  
1077 transient receptor channel is important for *Toxoplasma gondii* growth. *Elife* 10.

1078 54. Nagamune K, Moreno SN, Chini EN, Sibley LD (2008) Calcium regulation and signaling in apicomplexan parasites.  
1079 *Subcell Biochem* 47: 70-81.

1080 55. Maldonado EN, Lemasters JJ (2014) ATP/ADP ratio, the missed connection between mitochondria and the Warburg  
1081 effect. *Mitochondrion* 19 Pt A: 78-84.

1082 56. Frenal K, Dubremetz JF, Lebrun M, Soldati-Favre D (2017) Gliding motility powers invasion and egress in Apicomplexa.  
1083 *Nat Rev Microbiol* 15: 645-660.

1084 57. Carruthers VB (2019) Interrupting *Toxoplasma*'s Regularly Scheduled Program of Egress. *Trends Parasitol* 35:  
1085 338-340.

1086 58. Stasic AJ, Dykes EJ, Cordeiro CD, Vella SA, Fazli MS, et al. (2021) Ca(2+) entry at the plasma membrane and uptake by  
1087 acidic stores is regulated by the activity of the V-H(+) -ATPase in *Toxoplasma gondii*. *Mol Microbiol*.

1088 59. Lemgruber L, Lupetti P, Martins-Duarte ES, De Souza W, Vommaro RC (2011) The organization of the wall filaments  
1089 and characterization of the matrix structures of *Toxoplasma gondii* cyst form. *Cell Microbiol* 13: 1920-1932.

1090 60. Tu V, Mayoral J, Sugi T, Tomita T, Han B, et al. (2019) Enrichment and Proteomic Characterization of the Cyst Wall  
1091 from In Vitro *Toxoplasma gondii* Cysts. *mBio* 10.

1092 61. Zhang YW, Halonen SK, Ma YF, Wittner M, Weiss LM (2001) Initial characterization of CST1, a *Toxoplasma gondii* cyst  
1093 wall glycoprotein. *Infect Immun* 69: 501-507.

1094 62. Tomita T, Bzik DJ, Ma YF, Fox BA, Markillie LM, et al. (2013) The *Toxoplasma gondii* cyst wall protein CST1 is critical for  
1095 cyst wall integrity and promotes bradyzoite persistence. *PLoS Pathog* 9: e1003823.

1096 63. Tomita T, Sugi T, Yakubu R, Tu V, Ma Y, et al. (2017) Making Home Sweet and Sturdy: *Toxoplasma gondii* ppGalNAc-Ts  
1097 Glycosylate in Hierarchical Order and Confer Cyst Wall Rigidity. *mBio* 8.

1098 64. Dubey JP (1998) Re-examination of resistance of *Toxoplasma gondii* tachyzoites and bradyzoites to pepsin and  
1099 trypsin digestion. *Parasitology* 116: 43-50.

1100 65. Lin SS, Blume M, von Ahsen N, Gross U, Bohne W (2011) Extracellular *Toxoplasma gondii* tachyzoites do not require  
1101 carbon source uptake for ATP maintenance, gliding motility and invasion in the first hour of their extracellular  
1102 life. *Int J Parasitol* 41: 835-841.

1103 66. Blume M, Rodriguez-Contreras D, Landfear S, Fleige T, Soldati-Favre D, et al. (2009) Host-derived glucose and its  
1104 transporter in the obligate intracellular pathogen *Toxoplasma gondii* are dispensable by glutaminolysis. *Proc  
1105 Natl Acad Sci U S A* 106: 12998-13003.

1106 67. MacRae JI, Sheiner L, Nahid A, Tonkin C, Striepen B, et al. (2012) Mitochondrial metabolism of glucose and  
1107 glutamine is required for intracellular growth of *Toxoplasma gondii*. *Cell Host Microbe* 12: 682-692.

1108 68. Cardenas C, Miller RA, Smith I, Bui T, Molgo J, et al. (2010) Essential regulation of cell bioenergetics by constitutive  
1109 InsP3 receptor Ca2+ transfer to mitochondria. *Cell* 142: 270-283.

1110 69. Gherardi G, Monticelli H, Rizzuto R, Mammucari C (2020) The Mitochondrial Ca(2+) Uptake and the Fine-Tuning of  
1111 Aerobic Metabolism. *Front Physiol* 11: 554904.

1112 70. Pang X, Halaly T, Crane O, Keilin T, Keren-Keiserman A, et al. (2007) Involvement of calcium signalling in dormancy  
1113 release of grape buds. *J Exp Bot* 58: 3249-3262.

1114 71. Steinhorst L, Kudla J (2013) Calcium - a central regulator of pollen germination and tube growth. *Biochim Biophys  
1115 Acta* 1833: 1573-1581.

1116 72. Humeau J, Bravo-San Pedro JM, Vitale I, Nunez L, Villalobos C, et al. (2018) Calcium signaling and cell cycle:  
1117 Progression or death. *Cell Calcium* 70: 3-15.

1118 73. Nance JP, Vannella KM, Worth D, David C, Carter D, et al. (2012) Chitinase dependent control of protozoan cyst  
1119 burden in the brain. *PLoS Pathog* 8: e1002990.

1120 74. Nadipuram SM, Thind AC, Rayatpisheh S, Wohlschlegel JA, Bradley PJ (2020) Proximity biotinylation reveals novel  
1121 secreted dense granule proteins of *Toxoplasma gondii* bradyzoites. *PLoS One* 15: e0232552.

1122 75. Dzierszinski F, Nishi M, Ouko L, Roos DS (2004) Dynamics of *Toxoplasma gondii* differentiation. *Eukaryot Cell* 3:  
1123 992-1003.

1124 76. Tobin CM, Knoll LJ (2012) A patatin-like protein protects *Toxoplasma gondii* from degradation in a nitric  
1125 oxide-dependent manner. *Infect Immun* 80: 55-61.

1126 77. Wang ZT, Harmon S, O'Malley KL, Sibley LD (2015) Reassessment of the role of aromatic amino acid hydroxylases and  
1127 the effect of infection by *Toxoplasma gondii* on host dopamine. *Infect Immun* 83: 1039-1047.

1128 78. Carruthers VB, Giddings OK, Sibley LD (1999) Secretion of micronemal proteins is associated with *Toxoplasma*  
1129 invasion of host cells. *Cell Microbiol* 1: 225-236.

1130 79. Alagaran A, Fentress SJ, Tang K, Wang Q, Sibley LD (2013) *Toxoplasma* GRA7 effector increases turnover of  
1131 immunity-related GTPases and contributes to acute virulence in the mouse. *Proc Natl Acad Sci (USA)* 111:  
1132 1126-1131.

1133 80. Shen B, Brown K, Long S, Sibley LD (2017) Development of CRISPR/Cas9 for Efficient Genome Editing in *Toxoplasma*  
1134 *gondii*. *Methods Mol Biol* 1498: 79-103.

1135 81. Shen B, Brown KM, Lee TD, Sibley LD (2014) Efficient gene disruption in diverse strains of *Toxoplasma gondii* using  
1136 CRISPR/CAS9. *mBio* 13;5(3):e01114-14.

1137 82. Livak KJ, Schmittgen TD (2001) Analysis of relative gene expression data using real-time quantitative PCR and the  
1138 2(-delta-delta C(T)) method. *Methods* 25: 402-408.

1139 83. Menegollo M, Tessari I, Bubacco L, Szabadkai G (2019) Determination of ATP, ADP, and AMP Levels by  
1140 Reversed-Phase High-Performance Liquid Chromatography in Cultured Cells. *Methods Mol Biol* 1925: 223-232.

1141